THE UNIVERSITY of EDINBURGH

Edinburgh Research Explorer

Increasing the physical representation of forest-snow processes in coarseresolution models: lessons learned from upscaling hyper-resolution simulations

Citation for published version:
Mazzotti, G, Webster, C, Essery, R & Jonas, T 2021, 'Increasing the physical representation of forest-snow processes in coarseresolution models: lessons learned from upscaling hyper-resolution simulations', *Water Resources Research*, vol. 57, no. 5, e2020WR029064. https://doi.org/10.1029/2020WR029064 Read the full text

Digital Object Identifier (DOI):
10.1029/2020WR029064 Read the full text

Link:
Link to publication record in Edinburgh Research Explorer

Document Version:
Peer reviewed version

Published In:
Water Resources Research

General rights
Copyright for the publications made accessible via the Edinburgh Research Explorer is retained by the author(s) and / or other copyright owners and it is a condition of accessing these publications that users recognise and abide by the legal requirements associated with these rights.

Take down policy
The University of Edinburgh has made every reasonable effort to ensure that Edinburgh Research Explorer content complies with UK legislation. If you believe that the public display of this file breaches copyright please contact openaccess@ed.ac.uk providing details, and we will remove access to the work immediately and investigate your claim.

Download date: 06. May. 2023

Increasing the physical representation of forest-snow processes in coarse-resolution models: lessons learned from upscaling hyper-resolution simulations

Giulia Mazzotti[1,2], Clare Webster[1], Richard Essery[3], Tobias Jonas[1]

[1] WSL Institute for Snow and Avalanche Research SLF, Davos Dorf, Switzerland
[2] Laboratory of Hydraulics, Hydrology and Glaciology, ETHZ, Zurich, Switzerland
[3] School of Geosciences, University of Edinburgh, Edinburgh, UK

* Correspondence to: G. Mazzotti, giulia.mazzotti@slf.ch

Key points:

- Upscaling experiments with a well-validated hyper-resolution forest snow model allowed assessing process representation at coarse resolution
- Process-specific canopy metrics and detailed representation of shortwave radiation transfer improved coarse-resolution simulations
- Accounting for fractional snow-covered area is critical to simulating accurate melt rates even for relatively small grid cells

Abstract

Processes shaping forest snow cover evolution often vary at small spatial scales which are not resolved by most model applications. Representing this variability at larger scales and coarser model resolutions constitutes a major challenge for model developers. In this study, we use a well-validated hyper-resolution forest snow model that explicitly resolves the spatial variability of canopy-snow interactions at the meter scale to explore adequate representation of forest-snow processes at coarser resolutions (50m). For this purpose, we assess coarser-resolution runs against spatially averaged results from corresponding hyper-resolution simulations over a 150 000 m^2 model domain. For the coarser-resolution simulations, we tested alternative upscaling strategies. Our results reveal considerable discrepancies between strategies that utilize generalized canopy metrics versus strategies that apply a more detailed set of process-specific canopy descriptors. Particularly, the inclusion of canopy descriptors that represent the various scales and perspectives relevant to the individual processes leads to accurate simulation of forest snow cover dynamics at coarse resolutions. Our results further demonstrate that a realistic representation of snow-covered fraction in snowmelt calculations is important even for relatively small (~50 m) grid cells. Ultimately, this work provides recommendations for modelling forest-snow processes in large-scale applications, which allow coarse-resolution simulations to approximate spatially averaged results of corresponding hyper-resolution simulations.

1. Introduction

Accurate modelling of snow accumulation and melt processes under forest canopy is relevant for a variety of applications across a wide range of spatial scales. At the stand scale, the presence and duration of snow impacts eco-physiological and biogeochemical processes such as vegetation growth and microbial decomposition (Sorensen et al., 2016; Wipf & Rixen, 2010). At watershed scales, seasonal snow and its depletion in spring create distinct runoff patterns (Barnhart et al., 2016; Viviroli & Weingartner, 2004). In the Northern hemisphere, forest covers 19% of the seasonally snow-covered land surface (Rutter et al., 2009), making forest snow an important determinant of wintertime land surface albedo in these environments, with further influences on global-scale climate feedback mechanisms (Abe et al., 2017; Thackeray et al., 2014). In today's changing environment, both snow regimes and vegetation cover are subject to shifts (Derksen & Brown, 2012; Mote et al., 2018; Pearson et al., 2013): Consistent and dramatic snow cover declines have been reported, with decreases in June snow cover extents of ~13% per decade in arctic regions (Meredith et al., 2019) and reductions in snow cover duration of on average five days per decade at low elevations of alpine regions (Hock et al., 2019) since the 1960ies. These trends are expected to continue. Warming temperatures are further intensifying wildfire risk and insect outbreaks, causing a threat to boreal and mountain forest health (Gauthier et al., 2015). Reliable forest snow models can help us to better predict the consequences of these environmental changes. This is paramount in support of ecosystem and water management and further mitigation and adaptation strategies (Sturm et al., 2017; Viviroli et al., 2011).

Modelling forest snow remains challenging. The forest snow model intercomparison project SnowMIP2 demonstrated most snow models to perform worse in forests than in open areas (Essery

et al., 2009; Rutter et al., 2009). Forest snow cover dynamics are shaped by canopy-induced processes, including snow interception, radiation transfer, and wind attenuation (Moeser et al., 2015a; Musselman et al., 2012b; Roth & Nolin, 2017; Webster et al., 2016b). All these processes are strongly controlled by the structure of the forest canopy at small spatial scales and interact in various non-linear manners, creating a highly heterogeneous snow distribution. The true spatial variability of forest-snow processes can hence only be explicitly resolved in models operating at extremely high ('hyper') spatial resolutions (<5 m), which is unfeasible in most modelling applications (Clark et al., 2011). Model applications thus typically use coarser resolutions, where 'coarse' implies that grid cells size exceeds the spatial scale at which processes vary and interact. In case of forest-snow processes, 'coarse' can mean resolutions as small as 50 m based on scale breaks identified in earlier studies (Clark et al., 2011; Trujillo et al., 2009). It is still unclear how accurately existing parameterizations represent grid cell averaged snow cover dynamics at these resolutions, given that these were mostly developed and/or tested at the site scale (Gouttevin et al., 2015; Hedstrom & Pomeroy, 1998; Mahat et al., 2013).

Traditionally, many coarse-resolution models represent canopy structure in terms of generalized canopy metrics, usually Leaf Area Index (LAI), canopy cover fraction (CC), and mean canopy height (mCH), even if specific process parametrizations may vary (e.g. Bartlett & Verseghy, 2015; Best et al., 2011; Förster et al., 2018; Oleson et al., 2013). While individual grid cells may include multiple tiles characterized by different vegetation types, small-scale forest structure heterogeneities and their impact on directional processes are unaccounted for. Recent research suggests that such 'big-leaf' approaches fail to capture important effects of common forest-structural heterogeneities such as gaps, potentially leading to biased simulations of snow dynamics at coarse grid scales (Broxton et al., 2015; Essery et al., 2009; Moeser et al., 2016). In particular, this hypothesis is supported by experimental studies that demonstrated the control of local canopy structure characteristics on the small-scale variability of processes such as interception and short- and longwave irradiance, especially across canopy discontinuities (Lawler & Link, 2011; Moeser et al., 2015a; Webster et al., 2016a). Consequently, some developers of hydrological models have started to subdivide model units to separately represent strata such as forest and forest gaps (Ellis et al., 2013; Sun et al., 2018). In land surface models, recent advancements in radiative transfer schemes now allow discriminating shaded and sunlit canopy elements and accounting for canopy clumping and gap probabilities (Dai et al., 2004; Ni-Meister et al., 2010; Widlowski et al., 2015). However, it remains to be tested whether these approaches considerably improve simulations of snow water equivalent (SWE) over coarse grid scales in real-world applications with heterogenous forest cover.

In general, improvement of forest-snow process models suitable for coarse-scale applications is limited by the lack of appropriate experimental data. While extensive spatially-distributed snow depth datasets are becoming increasingly available from airborne lidar (Currier et al., 2019; Harpold et al., 2014; Mazzotti et al., 2019a; Painter et al., 2016), they do not resolve individual forest-snow processes and often lack temporal resolution to reflect single accumulation and/or ablation events. In contrast, experimental data intended to study individual forest-snow processes typically lack spatial resolution and coverage to be conclusive for model testing beyond the site

scale (Lundquist et al., 2013; Moeser et al. 2015a; Musselman et al., 2012a). For coarse-scale applications, the spatial mismatch between the extent of available measurements and the resolution at which processes need to be represented hampers effective model validation (Bloeschl, 1999; Essery et al., 2009). Yet, process-specific data would be essential to specifically assess the suitability of a canopy representation and its impact on individual processes, rather than to evaluate the combined effect of canopy and snowpack schemes (Mazzotti et al., 2020a).

With increased availability of high-quality canopy structure information from remotely-sensed datasets and improved processing algorithms, accounting for more detailed and realistic canopy structural features in large scale models has become a realistic option (Essery et al., 2008; Webster et al., 2020; Yuan et al., 2014). This opportunity has motivated efforts to develop hyper-resolution models that explicitly resolve forest-snow process variability. Broxton et al. (2015) introduced the forest snow model Snow Physics and Lidar Mapping (SnowPALM), which operates at 1 m resolution and has since been used to explore the effect of forest disturbances on snow water resources (Harpold et al., 2020; Krogh et al., 2020). The Factorial Snow Model (FSM; Essery, 2015), a medium-complexity snowpack energy balance model with a one-layer canopy, was also recently adapted for hyper-resolution forest snow simulations (now 'Flexible' Snow Model, FSM2; Mazzotti et al., 2020a,b). By diversifying the canopy structure metrics used in the individual process parametrizations, FSM2 accounts for the different canopy scales and perspectives relevant to the different processes (e.g. vertical vs. hemispherical), while maintaining compatibility with typical land surface model structures. Beyond reproducing observed snow depth patterns, the authors could demonstrate FSM2's ability to replicate small-scale spatial variations in energy fluxes to the forest snowpack using novel distributed multi-sensor datasets (Mazzotti et al., 2020b). Their study constituted a first extensive and spatially explicit process-level evaluation of a hyper-resolution forest snow model.

A major motivation for these efforts has been that well-validated hyper-resolution models can potentially help bridge the gap between the limited spatial coverage of process-level observations and the spatial extent of typical model grid cells (Mazzotti et al., 2020b). Hyper-resolution simulations provide fully-resolved, consistent estimates of the spatial variability of all involved processes in replacement of equivalent experimental data. They can thus be used to explore how small-scale forest-snow processes scale to coarser model resolutions at which their variability must be treated implicitly. To our knowledge, such an application has not been exploited to date: only Broxton et al. (2015) presented a brief analysis of the impact of model resolution on simulated snow water resources. They found degraded performance of SnowPALM at 100 m resolution relative to 1 m resolution, yet this result constituted only a minor part of their analysis.

This study leverages hyper-resolution simulations to advance the physical representation of forest-snow processes in coarser-resolution models. To this end, we perform model upscaling experiments with FSM2, building on the work presented by Mazzotti et al., (2020a,b). Our coarse-resolution simulations represent 50 m grid cells with one model run each. We assess different upscaling strategies by testing how such coarse-resolution simulations are affected by (1) implicit representation of canopy structure heterogeneity (2) implicit representation of snowpack

heterogeneity, and (3) consideration of spatial dependencies between the two. These simulations are evaluated against corresponding hyper-resolution simulations, the results of which are used in replacement of meter-scale observational datasets. Under this premise, hyper-resolution simulations will provide the "true" spatial mean of any model variable when aggregated over the same grid cells. While our controlled upscaling experiments do not yield a user-ready modelling framework, they allow us to derive recommendations for optimally representing forest-snow processes in coarser-resolution model applications.

2. Methods

This study builds on datasets and methods presented in earlier work by Mazzotti et al. (2020a,b) and Webster et al. (2020). Relevant data and modelling approaches are briefly summarized in the following, further technical details are available in the Appendix.

2.1 Study areas and data

Data were collected at two sites with variable forest structure (Figure 1): The first, located in the vicinity of Davos Laret in the Eastern Swiss Alps, features predominantly Norway spruce (*picea abies*). The second, situated south of Sodankylä in Northern Finland, mainly consists of Scots pine (*pinus sylvestris*). Both sites have hosted numerous experimental studies on forest-snow processes before (e.g. Malle et al., 2019; Moeser et al., 2015b; Reid et al., 2013; Webster et al., 2016a). In particular, Mazzotti et al. (2020b) presented spatially distributed measurements of short- and longwave radiation, air and snow surface temperatures, co-registered to canopy structure and snow distribution information acquired at both these locations during the 2019 snow season. For their study, they established 13 experimental plots (Figure 1) each consisting of a grid formed by eight interlaced 40 m transects. Along these transects, micrometeorological data and up-looking hemispherical photographs were collected at approx. 1.5 m spacing using a handheld sensor assembly presented by Mazzotti et al. (2019b), yielding 240 surveyed points per plot. Position and orientation of the experimental plots were chosen to cover typical stand features such as gaps, dense canopy and forest edges. Corresponding datasets thus enabled a thorough assessment of hyper-resolution simulations of the seasonal snowpack with FSM2 across a variety of canopy structures and climatic conditions. In particular, the model runs could be validated at the level of individual energy balance components, demonstrating the excellent performance of FSM2 in capturing the spatiotemporal variability of individual processes and in replicating the resulting snow distributions at both study sites (see Mazzotti et al. (2020b) for further details).

In this study, we use canopy structure data acquired at these experimental plots as basis for our model upscaling experiments. Meteorological input datasets required to drive FSM2 were assembled based on data from automatic weather stations located in forest clearings at both Laret and Sodankylä (Figure 1) as described in Mazzotti et al. (2020a,b). Upscaling experiments at these plots are complemented with simulations over a much larger 250 m x 600 m domain in Laret (in the following referred to as 'lidar domain', Figure 1), which coincides with the model domain from Webster et al. (2020). In their study, they used airborne lidar data available for the area (first presented by Moeser et al., 2014) to create synthetic hemispherical images at 1-m spacing. Point-

cloud enhancing techniques developed by the authors allowed for a realistic representation of canopy elements such as trunks and branches in these images, making them suitable to obtain sufficiently accurate estimates of the canopy properties needed to run FSM2 (see Section 2.2). Additional canopy structure input to FSM2 was derived from a canopy height model generated from the same lidar data (Mazzotti et al., 2020a).

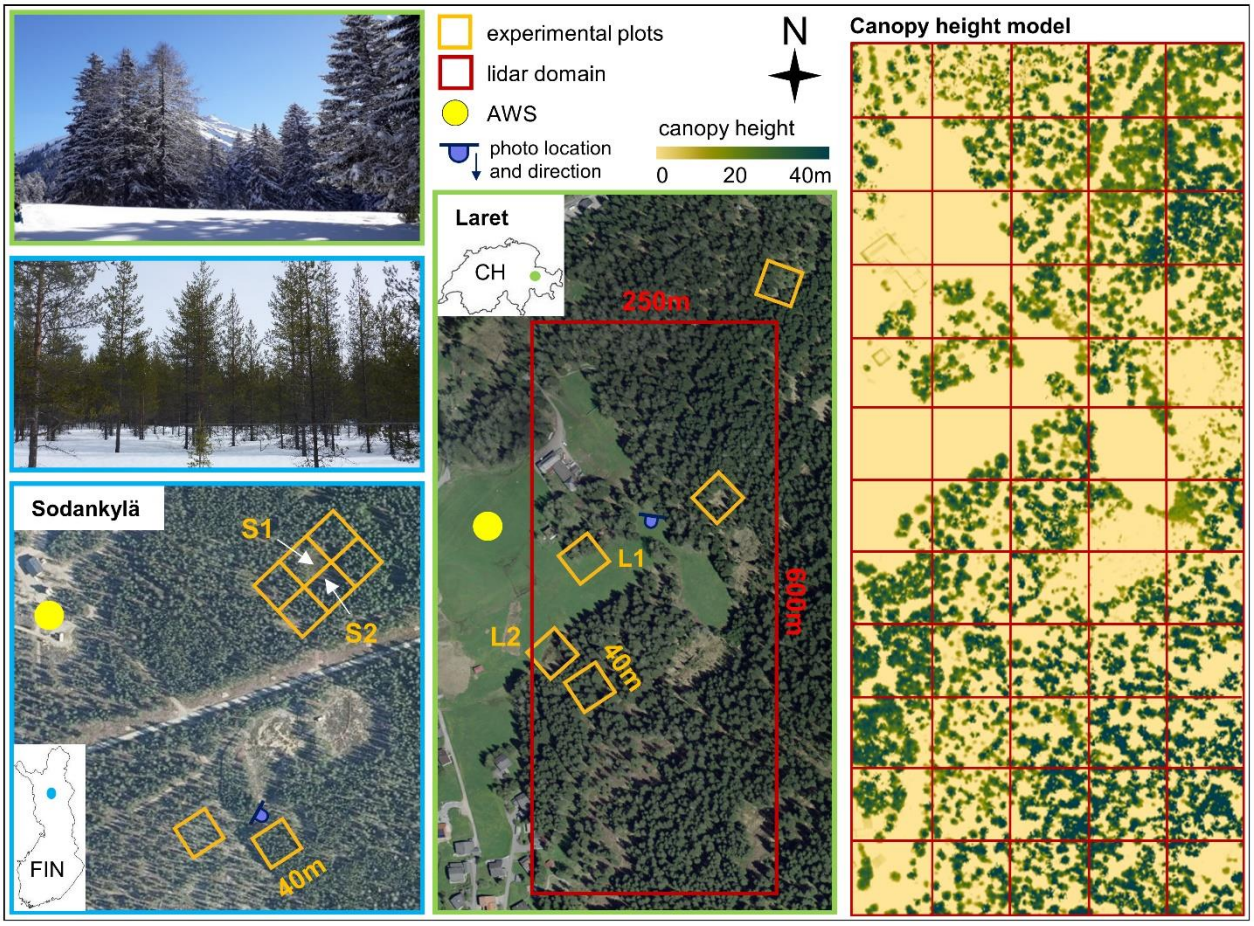

Figure 1: *Overview of study sites: aerial images of the forest sites at Sodankylä (Finland) and Laret (Switzerland), including locations of the experimental plots, the lidar model domain and automatic weather stations (AWS), and canopy height model of the lidar domain partitioned into 50 x 50 m grid cells.*

2.2 Concept of the modelling experiments

At the core of this study are upscaling experiments performed with the forest snow model FSM2, namely with the version specifically enhanced for hyper-resolution simulations (Mazzotti et al., 2020b). To date, this version of FSM2 is the only model capable of accurate hyper-resolution simulations that has been validated at the level of individual processes. Particularly, the model was shown to not only replicate detailed snow depth patterns, but also the complex spatiotemporal dynamics of internal fluxes (such as sub-canopy incoming short- and longwave radiation), as well as prognostic states (such as snow surface temperatures). Note that Mazzotti et al. (2020b) tested

their version of FSM2 at a variety of study sites including those considered here, so that the demonstrated model capabilities should apply to the simulations in this study.

The goal of our model experiments was to test the implicit representation of unresolved process variability in coarse-resolution simulations within an idealized framework. As the target for these experiments, we aggregated the results of hyper-resolution (2 m) simulations (described in Section 2.3) to yield their spatial means within 50 m resolution grid cells. Ideally, the coarse-resolution simulations would perfectly replicate the spatially averaged results of the corresponding hyper-resolution simulations.

The use of a hyper-resolution model framework enables thorough testing of various strategies to yield accurate coarse-resolution simulations (hereafter referred to as 'upscaling strategies'). Below-canopy shortwave radiation may provide an illustrative example: In principle, a radiation transfer scheme that can approximate the aggregated sub-canopy radiation output of hyper-resolution simulations should provide the best grid-cell scale estimate. Yet, in case of partial snow cover, the area in the grid cell with remaining snow may, in fact, receive less radiation than the grid cell average. This consideration suggests two alternative upscaling strategies: using a radiation transfer scheme that is trained to either replicate below-canopy incoming shortwave radiation averaged over the entire grid cell, or averaged only over the part of a grid cell that is still snow-covered. While we acknowledge that the latter strategy may be difficult to achieve, our upscaling experiments reveal whether the effort is necessary, or whether such non-linear interactions between model components can be neglected.

Another important aspect of using hyper resolution model simulations for upscaling experiments is that we can prescribe 'observed' states to avoid results being confounded by biased parameterizations. Reusing the above example, we could test upscaling strategies that include fractional snow cover, without being affected by uncertainties that existing parameterizations of snow-covered fraction may suffer from.

Figure 2 gives a conceptual overview of our model upscaling experiments. We analyzed four alternative upscaling strategies (detailed in Section 2.4) involving model features of increasing complexity. We assessed each strategy based on simple snow season descriptors that could be computed consistently for all grid cells and WYs, characterizing both accumulation and ablation processes (e.g. peak SWE and snowmelt during ablation period). Note that our upscaling experiments were not aimed at providing a user-ready coarse-resolution forest snow modelling framework. Rather they served to identify which coarse-resolution model strategy offers an optimal tradeoff between model requirements and model performance. The analysis will allow us to derive recommendations for future model development and application.

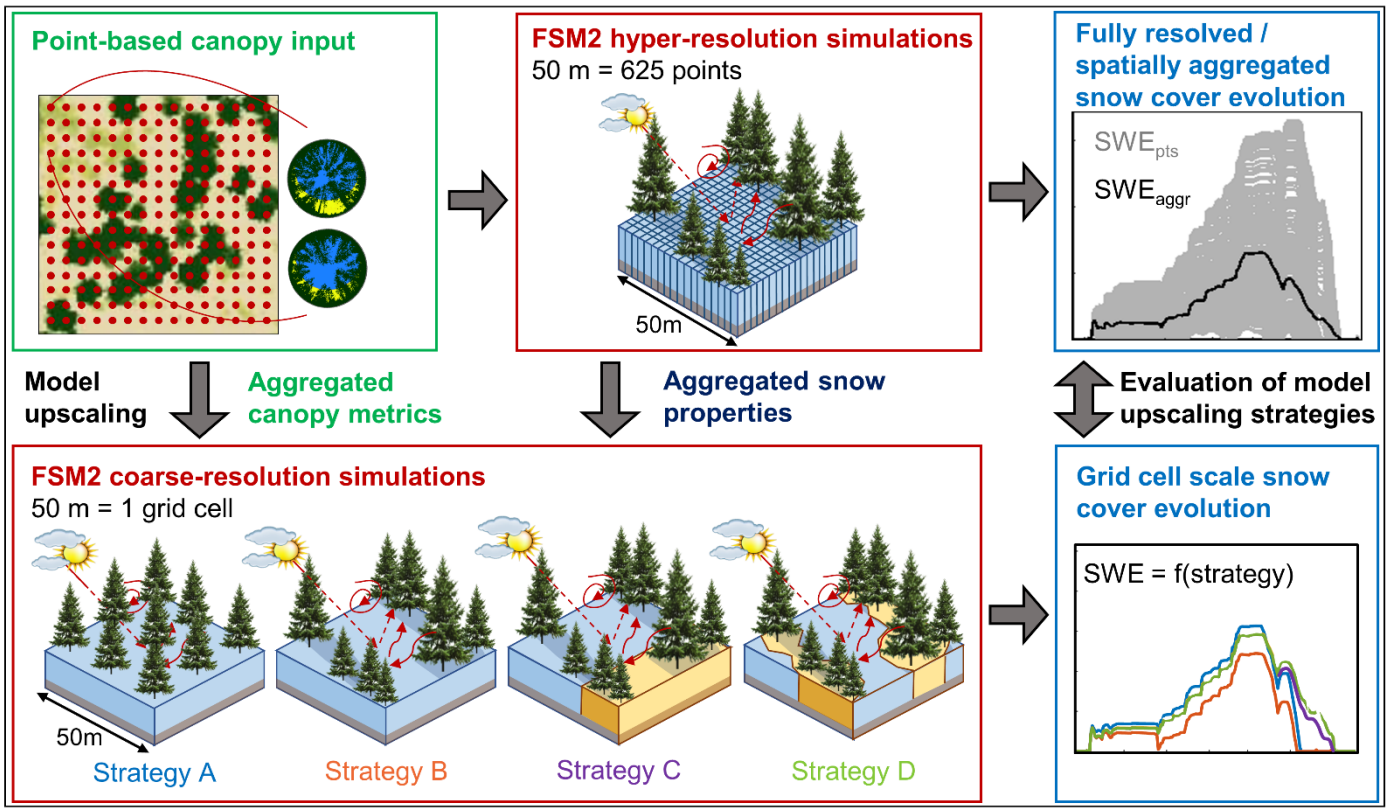

Figure 2: *Conceptual overview of the modelling experiments and analysis workflow, illustrated on an example grid cell from the lidar domain. Canopy properties used as input to the hyper-resolution simulations (Section 2.3) are computed from a canopy height model and synthetic hemispherical images. Snow water equivalent (SWE) output from the hyper-resolution model runs is averaged for comparison with results of the coarse-resolution simulations obtained with different strategies (Section 2.4). Aggregated canopy and snow properties input for the coarse-resolution runs are obtained from the hyper-resolution modelling framework.*

2.3 Hyper-resolution simulations

Our hyper-resolution simulations are essentially point simulations at 2-m spacing, for which FSM2 requires point-based canopy structure metrics. Mazzotti et al. (2020a,b) showed that integration of canopy structure metrics tailored to each individual process was key to obtaining an accurate representation of the forest snowpack at this resolution. Canopy structure parameters, their data sources, and their uses within FSM2 are summarized in Table 1. For further details on the physics of the snow and canopy modules of FSM2, we refer the reader to Essery (2015) and Mazzotti et al. (2020a,b).

Table 1: *Point-specific canopy structure input required for hyper-resolution FSM2 simulations. Subscript numbers denote the radius around a point [m] over which the metric is evaluated. See appendix for additional details.*

Canopy metric	Description, canopy scale / perspective	Data source	Calculation method	Process / usage

CC_5	Local canopy cover fraction, vertically projected	Canopy height model	Mazzotti et al. 2020a	Interception; Partitioning of near and distant canopy
CC_{50}	Stand-scale canopy cover fraction, vertically projected	Canopy height model	Mazzotti et al. 2020a	Wind attenuation / turbulent exchange
mCH_{50}	Stand-scale canopy height	Canopy height model	Mazzotti et al. 2020a	Wind attenuation / turbulent exchange
LAI	Local Leaf Area Index	Parametrized from CC_5 and mCH_5	Mazzotti et al. 2020a	Interception and heat capacities of the canopy
V_F	Hemispherical sky-view fraction	Real / synthetic hemispherical image	Jonas et al. (2020) ; Webster et al. (2020)	Longwave and diffuse shortwave radiation transfer
$\tau_b(t)$	Time-varying transmissivity for direct solar radiation	Real / synthetic hemispherical image	Jonas et al. (2020) ; Webster et al. (2020)	Direct shortwave radiation transfer

Hyper-resolution simulations were performed for the experimental plots in Finland and Switzerland (Figure 1) for water year (WY) 2019. Further simulations were performed over the 150 000 m^2 lidar domain. These simulations included additional 37 500 model points and covered six WYs (2013 to 2015 and 2017 to 2019). The contiguous area was subdivided into sixty 50m grid cells yielding aggregation units for the upscaling experiments.

2.4 Model upscaling to coarser resolution

The four alternative model upscaling strategies considered here built upon each other and differed in how they account for unresolved heterogeneity of canopy and snowpack properties within a coarse-resolution grid cell (Figure 2). The specific model features and input requirements of each strategy are summarized in Table 2.

Table 2: *Upscaling strategies, features and required input. Canopy input was aggregated by arithmetic averaging of the corresponding hyper-resolution input. Snowpack input comprised grid cell properties derived from the hyper-resolution simulation.*

Upscaling strategy	**Underlying assumptions on grid cell properties**	**Required input on canopy properties**	**Required input on snowpack properties**
A	Homogeneous canopy, homogeneous snowpack	LAI, mCH_{50}	-
B	Heterogeneous canopy, homogeneous snowpack	LAI, CC_5, CC_{50}, mCH_{50}, V_F, $\tau_b(t)$	-
C	Heterogeneous canopy, heterogeneous snowpack, interactions ignored	LAI, CC_5, CC_{50}, mCH_{50}, V_F, $\tau_b(t)$	$f_{snow}(t)$
D	Heterogeneous canopy, heterogeneous snowpack, interactions accounted for	LAI, CC_5, CC_{50}, mCH_{50}, V_F, $\tau_b(t,f_{snow})$	$f_{snow}(t)$, $\alpha_s(t,f_{snow})$

Strategy A was intended to serve as a reference. Consequently, we reverted to a basic version of FSM2, which closely resembles standard canopy structure representations used in common coarse-resolution forest snow models such as CLM, CLASS and SUMMA. In this version, canopy processes are described in terms of LAI and canopy height, which corresponds to treating the canopy as a homogeneous layer. Model details can be found in Mazzotti et al. (2020a), who used the same version for baseline simulations (c.f. their scenario FSM2_A). In strategy A, the upscaling only consisted of aggregating local estimates for LAI to yield grid cell averaged values.

In **strategy B**, we used the full capabilities of FSM2 adapted for hyper-resolution simulations as presented in Mazzotti et al. (2020b). Similar to strategy A, upscaling only consisted of aggregating the canopy descriptors, but this time applied to all six canopy metrics required for the version of FSM2 used in this study (Table 2). By including time-varying transmissivity for direct beam shortwave radiation, strategy B implicitly acknowledged a heterogeneous canopy structure within each grid cell. However, since the version of FSM2 used here corresponds to a point model, this strategy still assumed the snow cover to be uniform over the entire grid cell.

Strategy C introduced a fractional snow cover, thereby modifying the structure of FSM2 from that of a point model to that of an actual grid cell model. Grid cell-scale snow-covered fraction (f_{snow}) determined from the hyper-resolution run was provided to FSM2 The area in the grid cell with remaining snow may at each time step. Melt energy was weighted by f_{snow}, similar to the model implementation in Luce et al. (1999). Note, that f_{snow} was only used to scale melt energy, without forcing the melt out date of the coarse resolution run to equal that of the hyper resolution simulations. Canopy metrics remained aggregated over the entire grid cell even in periods of fractional snow cover. Therefore, while this strategy accounted for the heterogeneity of both the canopy and the snowpack, spatial dependencies between the two were neglected.

Strategy D additionally incorporated the spatial dependencies between canopy and snowpack heterogeneities within each grid cell. As fractional snow cover evolves, the canopy structure controlling forest-snow processes above the remaining snow-covered area may no longer be accurately represented by grid cell averaged metrics. To account for such interactions, transmissivities for shortwave radiation (τ_b) and sub-canopy snow albedo (α_s) were adjusted to the snow-covered area, and only evaluated where and when the hyper-resolution model still contained snow (c.f. Table 2). As in strategy C, corresponding α_s values were based on results from the hyper-resolution run. This adjustment achieved a more accurate representation of shortwave radiation flux to the snow-covered fraction of a grid cell. Non-linearities in other interactions between forest-snow processes were not considered. But since shortwave radiation is a principal driver of the spatial variability of the subcanopy energy budget (Malle et al., 2019; Musselman et al., 2012b; Sicart et al., 2004), non-linearities related to this process were expected to have the highest impact on coarse-resolution simulations.

3. Results

In the following sections, we compare and assess the individual model upscaling strategies introduced above (Section 2.4). After a qualitative overview of the results for the experimental plots (Section 3.1), a more systematic assessment of the upscaling strategies was performed with the results for the lidar domain (Sections 3.2-3.4). These latter simulations included a larger number of grid cells and multiple winters with varying snow conditions. By contrasting two upscaling strategies at a time, we were able to analyze the impact of specific coarse-resolution model features individually.

3.1 Overall qualitative assessment of model upscaling strategies

Figure 3 compares results from all upscaling strategies to the hyper-resolution runs at the experimental plots, where, as a first overview, SWE at peak of winter (SWE_{max}) and snow disappearance date (SDD) are considered as descriptors of the SWE evolution. Differences to peak SWE from the aggregated hyper-resolution run were consistently largest for strategy A, but smaller (and similar) for all other upscaling strategies. The comparison of snow disappearance date revealed that models that do not account for snowpack heterogeneity (strategies A and B) melted too early at all sites, while snow disappearance date of both models that did (strategies C and D) were similar and matched the snow disappearance date of the hyper-resolution runs more closely.

Between-site differences were large, however, and not all plots conformed to these generalized observations. At plot L1 in Laret, for instance, strategy C melted much earlier than strategies A and D. This plot was located at a south-exposed forest edge (see Figure 1 for location). Consequently, direct insolation was a main driver of melt energy, which was underestimated by strategy A that was not set up to account for the directionality of direct shortwave radiation. However, the areas receiving most direct insolation also melted out first. As a result, computing melt energy based on plot-averaged canopy properties (strategy C) obviously led to overestimations of melt rates in the later stages of snowmelt. Only strategy D yielded accurate melt rates, by incorporating spatial dependencies between canopy and snow cover heterogeneities. For all other plots, however, strategies C and D produced basically identical results, indicating minor importance of non-linear effects at locations that are not particularly sun exposed. This even applied to a small forest gap (plot S1 in Sodankylä, Figure 1), where the effect of direct insolation in the northern part of the gap is counteracted by shading from the trees at the southern end of the gap. Finally, plot S2 was handled well by all four strategies, and results were close to the aggregated output of the hyper resolution run. These simulations were characterized by (1) cold winter and hence only negligible melt before peak SWE, and (2) steep melt rates and hence non-linear effects becoming effective only towards the very end of the season.

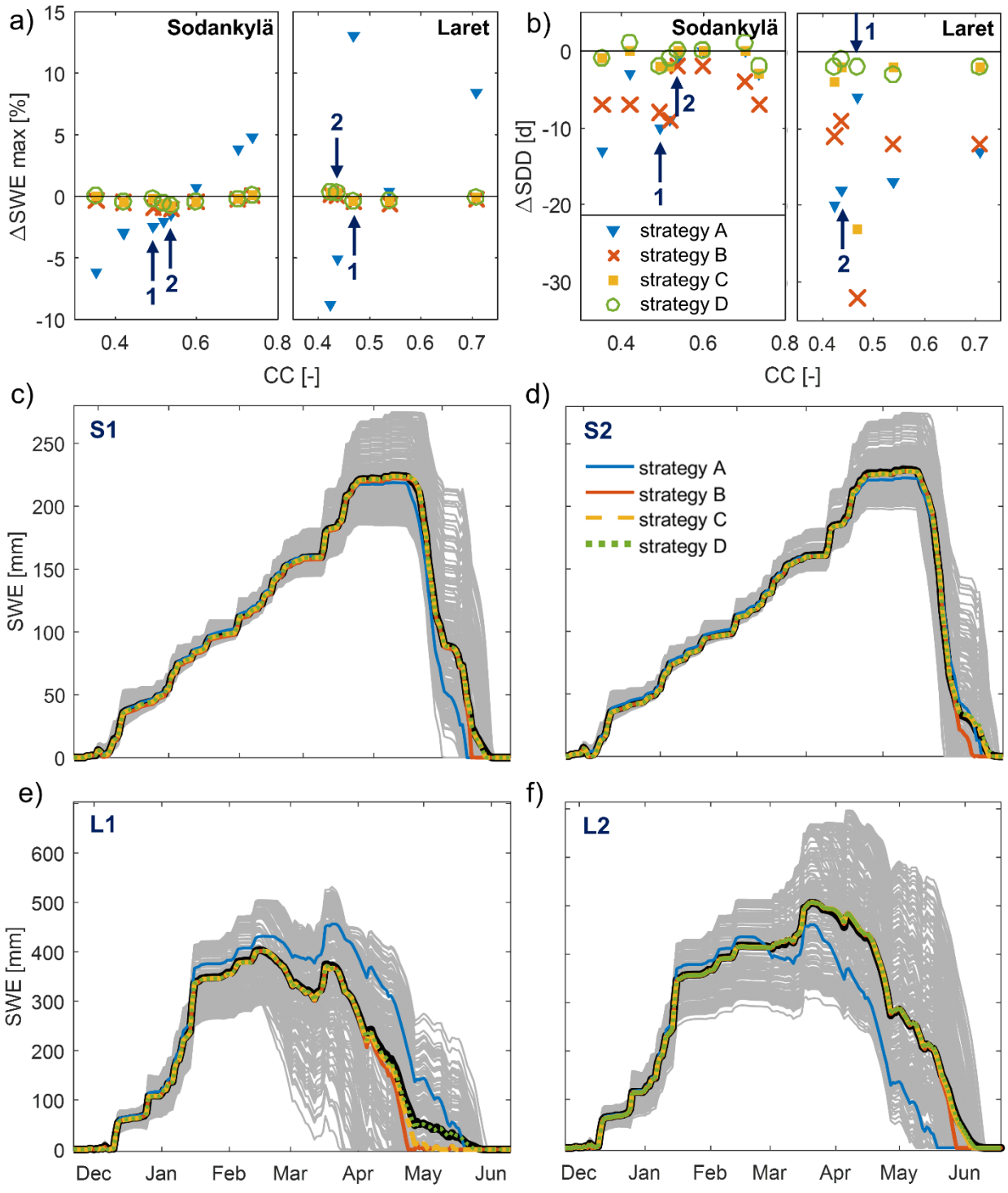

Figure 3: *Summary of results at the experimental plots: Difference in peak SWE (a) and snow disappearance date (b) between coarse- and hyper-resolution simulations as a function of plot-averaged canopy cover fraction (CC). Difference in peak SWE is expressed as percentage of the value predicted by the hyper-resolution runs, with positive/negative values denoting an overestimation/underestimation of peak SWE by the coarse-resolution runs. Accordingly, positive differences in SDD correspond to a later melt-out of the coarse-scale models. The SWE evolution*

plots (c to f, see Figure 1 for position) show individual points in hyper-resolution runs (grey lines) and their average (black lines) as well as coarse-resolution simulations with all strategies.

3.2 Impact of accounting for canopy structure heterogeneity (strategy A vs. B)

Strategies A and B differ in how canopy structure heterogeneity is accounted for, with impact on both accumulations and ablation processes. In comparison to the hyper-resolution simulations, strategy A mostly overestimated peak SWE (Figure 4a and b), the bias amounting to 5.6% on average with considerable differences between grid cells (Mean Absolute Error (MAE): 20.6 mm or 9.1%; Pearson's correlation coefficient (R): 0.96; both averaged over all WYs). Peak SWE obtained with strategy B, on the other hand, matched the hyper-resolution runs consistently well (Figure 4a and c), the average bias being -0.9% (MAE: 2.8 mm or 1.5%; R: 1.00). This substantial discrepancy between the two strategies arose because strategy A underestimated the range of peak SWE values across the lidar domain (Figure 4b, flatter slope than the 1:1 line for individual WYs).

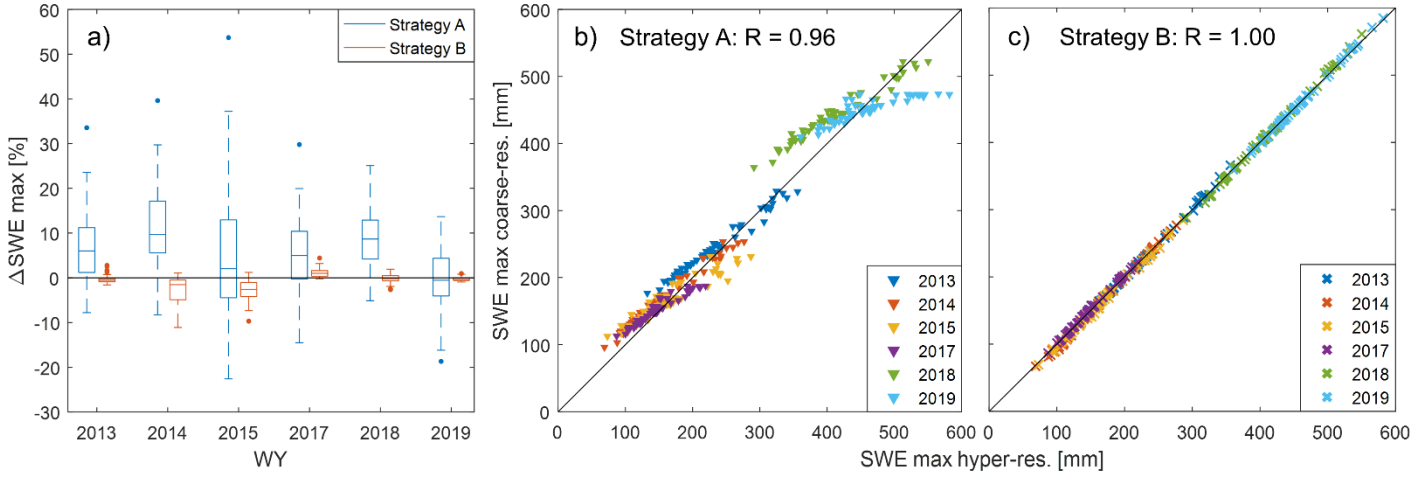

Figure 4: *Comparison of peak SWE simulated by upscaling strategies A and B across the lidar domain for all water years (WY): Differences in peak SWE between the averaged results of the hyper-resolution runs and of the two upscaling strategies (a) and peak SWE predicted by the hyper- vs. the coarse-resolution models for strategy A (b) vs. B (c).*

Both coarse-resolution model strategies consistently melted snow too early, on average by 11.4 and 10.9 days for A and B, respectively (Figure 5a). While snow disappearance date is the result of both accumulation and ablation dynamics, it is apparent that both strategies considerably overestimated melt rates, with a MAE of 48.6 mm (30%) for strategy A (Figure 5b), and a MAE of 30.7 mm (19%) for strategy B (Figure 5c). In case of strategy A, this bias was partly compensated by too high peak SWE values except in 2019 (c.f. Figures 4a and 5b). In comparison, melt rates from strategy B showed a much better correlation with respective results from the hyper-resolution simulations, but also with a systematic bias.

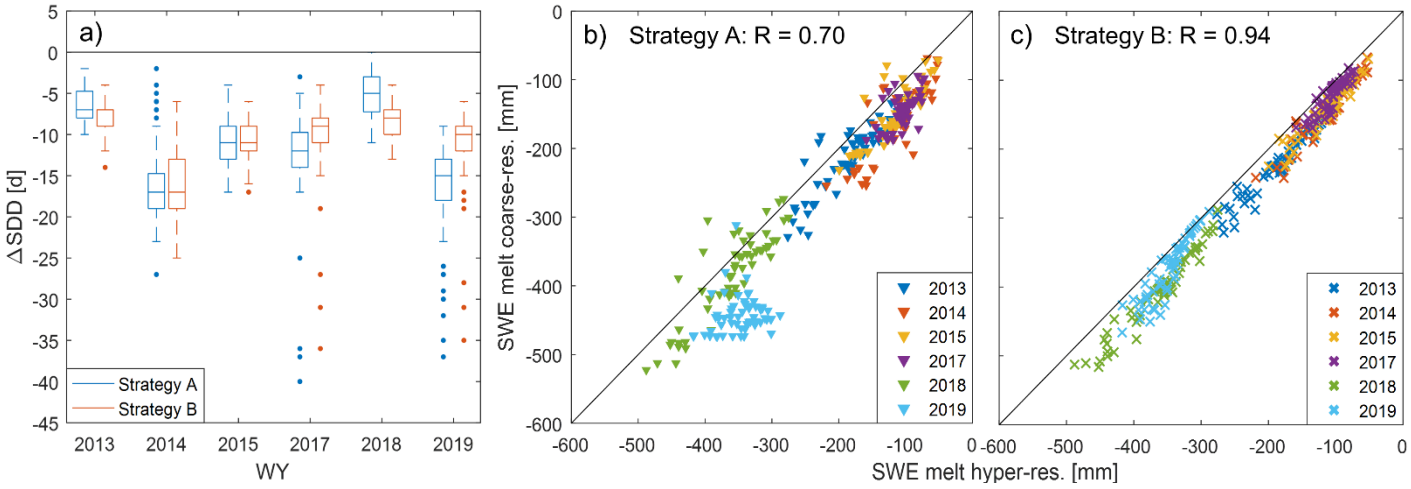

Figure 5: *Comparison of snow ablation simulated by strategies A and B, including* the *difference in snow disappearance date (SDD) between hyper- and coarse-resolution models (a) and corresponding difference in SWE melt for strategy A (b) and B (c). Melt was computed over the period between peak SWE and the earliest snow disappearance date of any of these three model versions.*

3.3 Impact of accounting for snowpack heterogeneity (strategy B vs. C)

Upscaling strategies B and C can only diverge in case of partial snow cover. While the snowpack in strategy B is treated as homogeneous across the grid cell, strategy C incorporates a snow-covered fraction which is used to scale the melt energy calculations. Differences to peak SWE predicted by the hyper-resolution runs were slightly larger in strategy C than in strategy B (bias of -0.9% vs 1.3%, MAE of 1.5% vs. 1.6%; Figure 6a). Note, that partial snow cover can already occur during the accumulation period. Figure 6b displays relative differences in peak SWE between strategies B and C as a function of partial snow cover occurrence before the date of peak SWE. Discrepancies between the hyper-resolution and the coarse-resolution simulations were indeed larger if partial snow cover occurred during a longer portion of the accumulation period (Figure 6b).

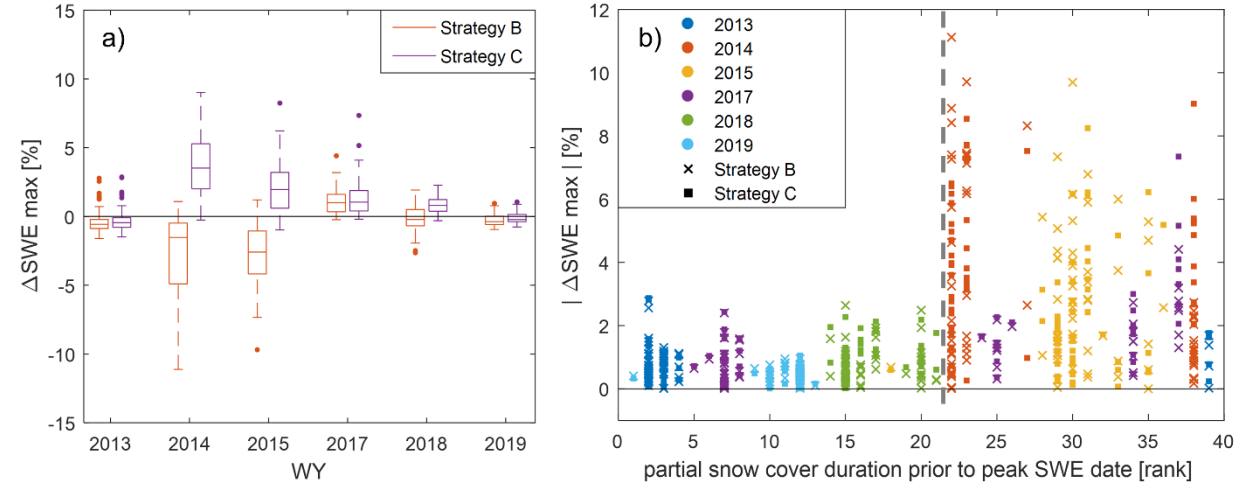

Figure 6: *Difference between peak SWE predicted by the averaged hyper-resolution runs and by upscaling strategies B and C (a) and Δ peak SWE plotted for individual grid cells as a function of partial snow cover duration during accumulation (b), both in relative terms. The snow cover duration is derived from the hyper resolution runs and ranked for better readability. The dashed line separates ranks corresponding to fractional snow during less and more than 50% of the accumulation period.*

The above deficiencies of strategy C in replicating peak SWE were minor compared to its higher accuracy in capturing ablation rates, which shows when contrasting discrepancies in peak SWE to biases in snowmelt in absolute terms (Figure 7). Across the lidar domain and over all modelled WYs, the average biases between peak SWE values predicted by the hyper-resolution runs and the coarse-resolution models amounted to -1.2 mm and 2.3 mm for strategies B and C, respectively (Figure 7a and d). The corresponding MAEs were 2.8 mm and 3.1 mm. As expected, ablation rates predicted by both upscaling strategies largely coincided while full snow cover was present (Figure 7b and e), and closely matched the hyper-resolution runs (bias: < 1 mm and MAE: 1.8 mm for both models). However, the two coarse-resolution models strongly diverged during partial snow cover: while strategy C and the hyper-resolution run still agreed well (bias: 1.9 mm; MAE: 3.6 mm), strategy B largely overestimated melt rate, with an average bias of -40.2 mm and 40.2 mm MAE (Figure 7c and f). These values clearly outweighed the small discrepancies in peak SWE estimates, and improved representation of snowmelt by strategy C was decisive to prevent the accelerated melt-out observed in strategy B (see Section 3.2).

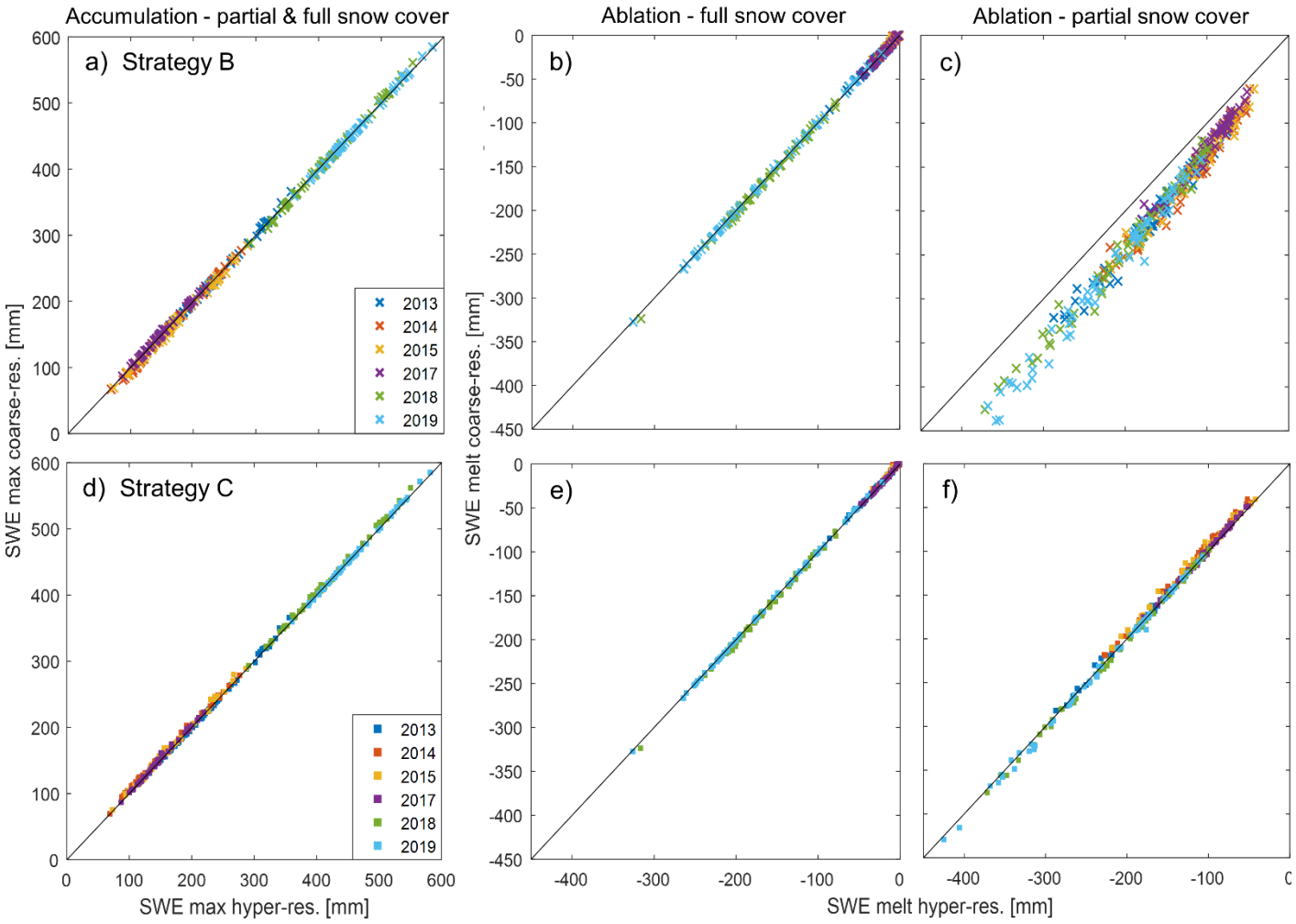

Figure 7: *Comparison of peak SWE (a, d) and melt during full (b, e) and partial (c, d) snow cover predicted by the hyper-resolution runs and strategies B (a-c) vs. C (d-f) across the entire lidar domain and for all simulated WY. As in Figure 5, melt was computed between peak SWE and the earliest snow disappearance date of any of these three model versions.*

3.4 Impact of accounting for non-linear interactions between canopy and snow heterogeneities (strategy C vs. D)

As a final comparison, Figure 8 contrasts strategies C and D. Both strategies implicitly represent canopy and snowpack heterogeneity, but only strategy D acknowledges spatial dependencies between the two heterogeneities by constraining shortwave radiation fluxes according to the remaining snow-covered area. Like in the previous comparison, strategies C and D can only diverge in situations with partial snow cover. Differences to the hyper-resolution run during both accumulation and ablation were only slightly reduced by accounting for non-linear effects, as the two strategies exhibited minor differences. As expected, the bias and MAE of peak SWE were almost identical (results not shown). Refining shortwave radiation fluxes in strategy D reduced the bias of snowmelt during partial snow cover conditions from 2.5 mm to 0.6 mm and the MAE from 5.3 to 3.3 mm, which in practical terms are negligible errors (Figure 8).

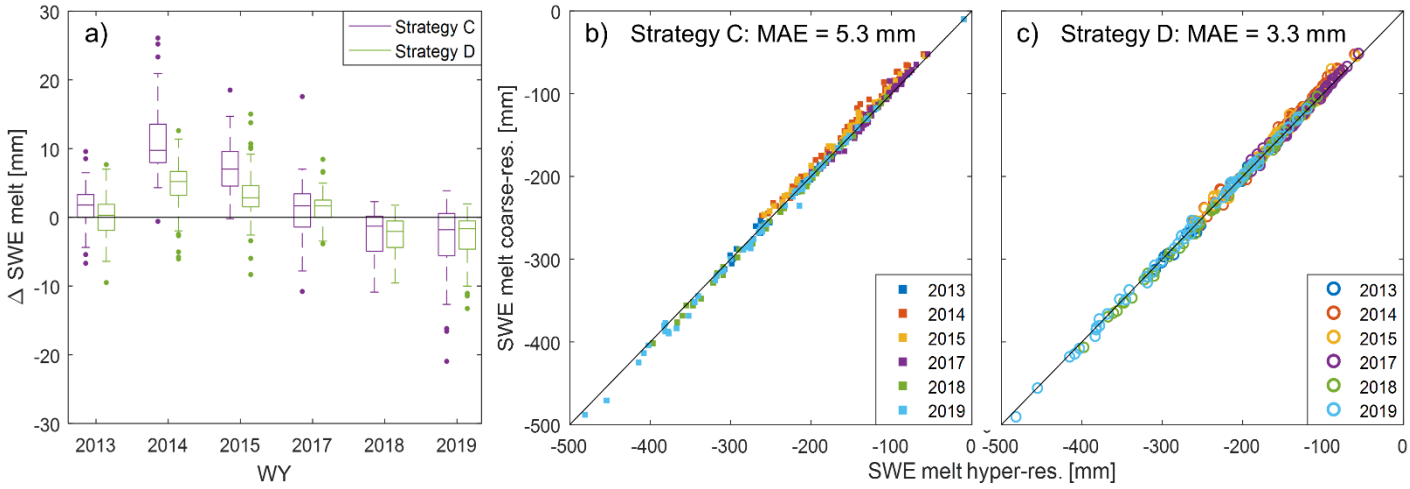

Figure 8: *Difference in SWE ablation during partial snow cover between the hyper-resolution runs and the upscaling strategies C and D (a), with positive differences denoting slower snow cover depletion in the coarse-resolution models. Comparison of melt during partial snow cover conditions predicted by the hyper- and coarse-resolution models, i.e. strategy C (b) and D (c). Melt was computed over the period between the onset of partial snow cover and the earliest snow disappearance date of any of these three model versions.*

Figure 8a further reveals that upscaling strategies C and D may both accelerate and delay melt-out depending on the year. We note that biases in ablation rate differ between winters, where coarse-resolution models tended to delay melt in WYs with shallow snowpacks (2014 and 2015). Ultimately, this indicates that the performance of each specific model upscaling strategy does not only depend on the site characteristics, but also on meteorological conditions, as the relative importance of processes governing snow cover evolution may vary between winters.

4. Discussion

Approaches to represent forest-snow processes in coarse-resolution models are difficult to verify against experimental data due to the spatial mismatch between observations, the scale of process variability, and typical model grid cell sizes. Consequently, insights from process-level experimental data are more easily implemented into point-scale models, which includes hyper-resolution models. Recent efforts in developing hyper-resolution models yielded the latest version of FSM2, which has been shown to capture realistic spatial variability of individual forest-snow processes (Mazzotti et al., 2020b). Simulations with FSM2 constituted a useful framework for testing coarse-resolution modelling approaches, providing reliable and consistent information on process variability typically unresolved in coarse-resolution simulation. Using hyper-resolution simulations as intermediary between real-world data and larger-scale models, the modelling experiments presented here allowed for a novel and systematic assessment of various model upscaling strategies, yielding insights that will benefit future large-scale forest snow modelling applications. As canopy structure controls on forest snow dynamics vary with climatic conditions (Currier & Lundquist, 2018; Lundquist et al., 2013; Varhola et al., 2010), our results should encourage the continued application of hyper-resolution models to investigate model upscaling

issues across a wider range of forest types and snow climates, and for even coarser model resolutions.

4.1 Relevance and implications of canopy structure heterogeneity

The comparison of strategies A and B demonstrated the benefit of accounting for canopy heterogeneity within coarse-resolution model grid cells by incorporating diversified rather than generalized canopy structure descriptors, as well as detailed shortwave radiation dynamics. The canopy representation applied in strategy A was used as a reference in this study, being equivalent to those used in many traditional models. It must, however, be pointed out that LAI values used here were derived based on values from the hyper-resolution runs to enable a consistent upscaling experiment. As these point-based LAI values scale with local canopy cover fraction (Mazzotti et al., 2020a), their aggregation over coarse-resolution grid cells yield LAI values that integrate a much higher level of detail than commonly applied LAI estimates. Coarse-resolution simulations based on available, less detailed LAI datasets (Faroux et al., 2013; Gichamo & Tarboton, 2020; Magnusson et al., 2019; Todt et al., 2019) were beyond the scope of this study but would likely diverge from simulations that use an enhanced canopy structure representation (strategy B) even more.

Nevertheless, when all process parametrizations rely on one or two generalized canopy density metrics (e.g. LAI in strategy A), the canopy scales and perspectives relevant to different processes cannot be sufficiently diversified, and directionality cannot be accounted for. Consequently, errors arise especially at locations where different process-specific metrics are uncorrelated (e.g. in canopy gaps, which can have $CC_5 = 0$ but $V_F < 1$). Mazzotti et al. (2020a,b) showed that a set of canopy metrics integrating diverse canopy scales and perspectives is needed to arrive at realistic hyper-resolution simulations. Yet, whether corresponding effects average out at coarser resolutions had not previously been investigated. Our results revealed that upscaled simulations indeed capture grid-cell averaged snow cover dynamics well, but only when fed with the same process-specific canopy structure metrics and time-varying direct beam transmissivities calculated at hyper-resolution and subsequently averaged across the grid cell. These findings highlight the importance of canopy structure heterogeneity for coarse-resolution modelling applications. They are in line with airborne lidar-based observations presented by Mazzotti et al. (2019a), who linked snow cover variability at aggregated spatial scales to the horizontal arrangement of canopy elements within grid cells.

Using spatially averaged time-varying transmissivities for direct shortwave radiation in coarse-resolution FSM2 simulations allows highly complex radiative transfer dynamics to be accounted for while maintaining a simple structure of the radiative transfer scheme in FSM2. Instead, an external radiative transfer model operating at much higher spatial and temporal resolution is tasked to provide this grid cell scale transmissivity input, which is essentially decoupling a remote sensing problem from the actual snow modelling. Outsourcing radiation modelling entails crucial benefits for operational applications: Computationally expensive

radiative transfer calculations can be conducted offline and one single time for use over multiple years of snowpack simulations without affecting real-time snow model applications. This procedure is possible as transmissivities for downwelling shortwave radiation are independent of the snow cover evolution, provided we ignore (1) the influence of canopy snow, and (2) interactions affecting the spatial aggregation of transmissivities addressed in strategy D. Both omissions have supposedly (1) or demonstrably (2) only a minor impact on the accuracy of the snow simulations, which clearly does not outweigh the benefits of this separation. Calculating detailed transmissivities, however, requires high-quality canopy datasets. Methods to extract such information from different datasets and for different forest types should be a priority of upcoming forest snow research.

4.2 Relevance and implications of snowpack heterogeneity

Neglecting unresolved snowpack variability in strategy B consistently overpredicted melt-out relative to the hyper-resolution run. This is a direct consequence of ignoring fractional snow cover in snowmelt calculations (Liston, 2004; Luce et al., 1999) and could be mitigated with strategy C. Notwithstanding, some studies have applied point models even for distributed simulations at coarser scales without consideration of sub-grid variability in forests (Cristea et al., 2014; Garen & Marks, 2005), while other models (including FSM in its original version, c.f. Essery, 2015) incorporate a parametrization of fractional snow cover but use it only to scale ground surface properties (Essery et al., 2013; Liston, 2004). These approaches are only adequate where snow distribution can be assumed to be approximately homogeneous over a grid cell, leading to a short duration of fractional snow cover throughout the snow season (e.g. as was the case for the Sodankylä plots). However, the strong variability of forest-snow processes can create substantial heterogeneities even within small grid cells, which implies that point-scale models have limited applicability in these environments.

To avoid accelerated melt-out and related errors in estimating e.g. streamflow magnitude and timing, forest snow models should therefore account for fractional snow cover even when operating with relatively small model grid cells. This enables scaling the melt rate with snow-covered fraction, which is only a first-order solution. A more rigorous approach should include separate energy balance calculations for snow-covered and snow-free fractions of the grid cells (Liston, 2004). Although some land surface models offer this capability (Boone et al., 2017; Swenson & Lawrence, 2012), only less than half of the models participating in SnowMIP2 actually did. Note, however, that implementing coupled energy balance equations over separate snow-covered and snow-free surfaces entails a substantial increase in model complexity.

In this study we were able to work with synthetic fractional snow cover data inherited from the hyper resolution simulations, thus representing the "correct" values. In real-world coarse-resolution applications, however, a snow-covered fraction parametrization is needed. But there is, to the best of our knowledge, a lack of dedicated approaches that describe snow cover fraction as a function of canopy structure metrics, which is surprising given how important this aspect is (Figure 7c vs 7f). Recently, fractional snow cover in forests has received some attention thanks to increased availability of extensive snow distribution data from airborne lidar: Kostadinov et al.

(2019) developed an approach to infer sub-canopy fractional snow cover from snow-covered area at open sites. However, as their study was motivated by the need to enhance other remotely sensed datasets over forested area, it did not address parametrizations that could be implemented into forest snow models. Snow cover depletion curves specific to forest tiles and grid cells have been used by DeBeer and Pomeroy (2017) based on coefficients of variation suggested by Liston (2004), but could not be verified against experimental data. In accordance with Dickerson-Lange et al. (2015) and Mazzotti et al. (2019a), our simulations suggest snow cover depletion curves that account for canopy structure to be a promising way forward because the distribution of peak SWE across the lidar domain was very consistent between years (mean correlation coefficient R = 0.98; results not shown). However, diverging results at the experimental plots in Laret and Sodanklyä imply that such parametrizations would need to account for climatic conditions as well. Future studies could combine spatially distributed forest snow datasets from repeated lidar flights (Broxton & van Leeuwen, 2020; Painter et al., 2016; Pflug & Lundquist, 2020) and hyper-resolution models to develop dedicated snow-covered fraction parametrizations for forested areas.

4.3 Synthesis and remaining challenges

With both canopy structure and snowpack heterogeneity implicitly accounted for, the snowpack evolution simulated by the hyper-resolution model could be well matched with coarse-resolution simulations. Further accounting for non-linear effects by constraining shortwave radiation fluxes (strategy D) added little benefit, with considerable impacts only in very specific canopy settings (e.g. Figure 3, example L1). But when evaluating simulations over six WY from a set of grid cells with a large range of canopy structure configurations, the spatial dependencies between canopy and snowpack heterogeneities were negligible (Figure 8). Strategy C thus represents a suitable tradeoff between model complexity and model performance. Figure 9 provides a visual evidence of this tradeoff, using data from WY 2019 as an example. The transition from basic to enhanced canopy representation (strategy A to B) mainly entails an improved representation of SWE variability at peak of winter, while the transition from an enhanced point to an enhanced grid cell model (strategy B to C) allowed for a more accurate prediction of melt-out timing. Insights from our model upscaling experiments are independent of the particular snow modelling framework used here and should hence apply to forest snow models other than FSM2 as well.

The largest discrepancies between hyper-resolution runs and upscaling strategies that implicitly represented both canopy and snowpack heterogeneities occurred when partial snow cover persisted throughout extended periods of the snow season. Patchy snowpacks are particularly challenging for coarse-scale models. These situations may require more complex approaches, such as tiling, to accurately represent snowpack dynamics in these situations. Further research is necessary to explore model upscaling strategies in forests that experience frequent mid-winter melt-out events or ephemeral snow, conditions which are expected to become more common in a warming climate (Contosta et al., 2019; Dickerson-Lange et al., 2017).

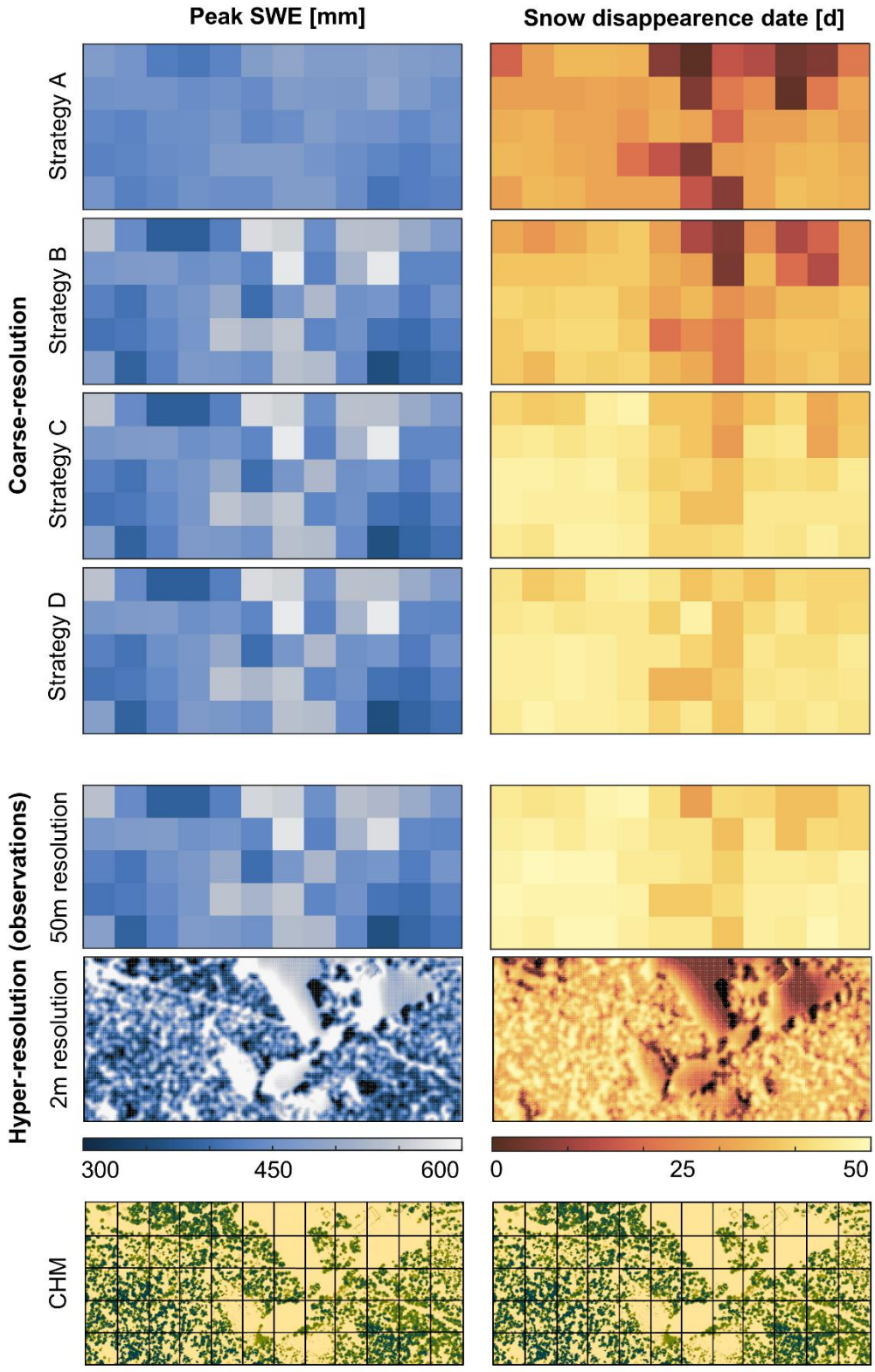

Figure 9: *Distribution of peak SWE (left) and snow disappearance day (right) in WY 2019 across the lidar domain as predicted by all upscaling strategies (rows 1-4) compared to the hyper-resolution run (rows 5-6). The canopy height model (c.f. Figure 1) is shown below for comparison.*

Note that all plots are oriented with North pointing right. Absolute values of snow disappearance day refer to the offset from the fist melt-out of any cell in any model version.

Remarkably, differences between the upscaling strategies were more pronounced at the Laret plots, and less distinct at the Sodankylä plots, although both sites featured plots with diverse canopy structure configurations. This underlines the importance of assessing upscaling strategies not only for a variety of canopy structure configurations, but also under varying climatic conditions. Future studies should further consider the combined impacts of topography and forest structure on snow cover heterogeneities in the context of model upscaling strategies.

5. Conclusion

This study has leveraged simulations obtained with a hyper-resolution model capable of explicitly resolving the small-scale variability of forest-snow processes to explore alternative strategies for the representation of these processes at coarser resolutions. Model upscaling experiments showed that integrating a detailed, process-specific canopy representation provides considerable improvements, even at coarser model resolutions. Further analysis revealed that snow disappearance occurs too early if fractional snow cover is unaccounted for in the energy balance calculations, even for relatively small grid cell sizes. With both canopy structure and snowpack heterogeneity implicitly accounted for, the coarse-resolution simulations achieve a close match to the spatially-averaged hyper-resolution runs. Additional consideration of further non-linear effects, such as the interaction between partial snow cover and shortwave radiation dynamics, improve the coarse-resolution simulations only minimally.

Our results highlight the potential of separating computationally intensive calculations of canopy radiative transfer properties from the snow cover modelling framework, allowing to integrate detailed canopy structure information into the snow model without compromising its computational efficiency. Obtaining corresponding datasets will soon be facilitated by the increasing availability of remote sensing products. Yet, continued efforts are needed to ensure the consistency of respective processing algorithms across forest and data types. Further research is also needed to address the development of fractional snow cover parametrizations that explicitly account for forest structure and climatic conditions. Implementation of these concepts will enable a more accurate representation of forest-snow processes in models intended for large scale applications, enhancing their ability to predict the impacts of ongoing environmental changes.

Acknowledgements

This study was funded by the Swiss National Science Foundation, project 200021_169213. Fieldwork in Sodankylä was partly funded by INTERACT under the European Union H2020 Grant Agreement No.871120 (project IME4Rad) and by NERC geophysical equipment facility loan 1108. FSM development is supported by NERC grant NE/P011926/1. We thank Steven Hancock, Benedikt Friedrich, Kalliopi Koutantou, Robin Maedel, Johanna Malle, and Nick Rutter for field support. We further thank the members of the SLF Snow Hydrology Group for insightful discussions on the topic of this manuscript, as well as Jessica Lundquist for helpful feedback on a

first draft. Finally, we acknowledge the efforts of three anonymous reviewers whose comments helped to improve this article. Documented code of FSM2 used for hyper-resolution simulations is available on GitHub (https://github.com/GiuliaMazzotti/FSM2/tree/hyres_enhanced_canopy). Data used in this study can be accessed on the Envidat repository (https://www.envidat.ch/dataset/chm-hp-4rtm).

Appendix

Concepts of FSM2 relevant to this work are summarized in the following. Rather than providing a full documentation of the model equations, the purpose of this appendix is to illustrate the use of canopy and snow properties relevant to the four model upscaling strategies. We refer to Mazzotti et al. (2020a,b) for further details on the canopy model, and to Essery et al. (2015) for details on the snow model. Note that thorough documentation of the model code is also available on the corresponding GitHub repositories.

FSM2 model structure, energy balance and canopy descriptors

FSM2 includes a one-layer canopy for forest snow simulations, i.e. the canopy is characterized by one state variable, vegetation temperature T_v. T_v is obtained by solving the coupled energy balances of the canopy and the snow surface at each time step, comprising an equation system with unknowns T_v, T_s (snow surface temperature), T_c (canopy air space temperature) and Q_c (canopy air space humidity). This model structure largely follows Bewley et al. (2010). The change in T_s at each time step determines energy flux into the snowpack, and once T_s reaches 0°C, the same set of equations yields energy available for snowmelt.

The flux parametrizations used in FSM2's energy balance are all taken from established land surface and/or snow hydrological models; what makes FSM2 particularly suited for hyper-resolution simulations is the use of diverse metrics within each process parametrization. This approach allows different canopy scales and perspectives relevant to different processes to be accounted for. In fact, the canopy structure descriptors listed in Table 1 comprise vertical and hemispherical perspectives, local and stand-scale, and include temporally static and dynamic ("time-varying") canopy properties. The use of individual metrics is detailed in the following.

Forest-snow process parametrizations using process-specific canopy descriptors

The most important canopy structure impacts on mass and energy fluxes to the sub-canopy snowpack include interception snow in the canopy, transmission of shortwave radiation through the canopy, emission of thermal (longwave) radiation by the canopy, and wind attenuation.

Interception of snowfall by the canopy follows Hedstrom & Pomeroy (1998). The increase in intercepted snow mass over timestep δt is:

$$\delta S_v = (S_{\max} - S_v)\left[1 - \exp\left(-\frac{f_v S_f \delta t}{S_{\max}}\right)\right]$$

Where S_v is intercepted snow mass at the beginning of the timestep, S_f is snowfall rate, and $S_{\max} = c_v \mathrm{LAI}$ is maximum canopy snow holding capacity (see Hedstrom & Pomeroy (1998) for species-specific values of cv). Because precipitation is an essentially vertical process and interception is strongly dependent on local canopy characteristics (Moeser et al. 2015a), FSM2 uses $f_v = CC_5$ and a local estimate of LAI (Table 1).

Sub-canopy irradiance at each specific location, in contrast, is dictated by canopy structure in the entire hemispherical field of view. Net shortwave radiation absorbed by the snow surface is:

$$SW_s = (1 - \alpha_s)(\tau_b SW_{\downarrow b} + \tau_d SW_{\downarrow d})$$

where $SW_\downarrow$ is the downwards shortwave radiation flux above the canopy split into direct-beam (b) and diffuse (d) components and α_s is snow albedo. Transmissivity of diffuse shortwave radiation τ_d corresponds to sky-view fraction (V_F, Table 1). Transmissivity for direct shortwave radiation τ_b is determined by canopy structure in the path of the solar beam and thus features a strong spatiotemporal dynamic. Time series of $\tau_b(t)$ at each point are obtained with external hemispherical-images based radiation transfer models based (Jonas et al. 2020, Webster et al. provided to FSM2 as input (Table 1).

Net longwave radiation at the snow surface is:

$$LW_s = \tau_{nc}(\tau_{fc} LW_\downarrow + (1 - \tau_{fc})\sigma T_a^4) + (1 - \tau_{nc})\sigma T_v^4 - \sigma T_s^4$$

where $LW_\downarrow$ is above-canopy incoming longwave radiation flux, and σ is the Stefan-Boltzmann constant. Canopy in the hemispherical view field is split into near and distant canopy elements with different temperatures, with distant canopy temperature approximated by air temperature T_a. Partitioning between near and distant canopy elements is constrained by V_F and CC_5: transmissivity of the near canopy elements is taken as $\tau_{nc} = 1 - f_v$, and near and far canopy transmissivities multiply to yield sky-view fraction: $\tau_{nc} * \tau_{fc} = V_F$.

Wind attenuation by the canopy affects turbulent exchange at the snow surface. Since canopy impacts on wind speed are less local than on interception, FSM2 uses stand-scale canopy structure metrics in the corresponding parametrization. Following Mahat et al. (2013), a composite profile (logarithmic decay above the canopy top at height h, exponential decay between h and a below-canopy level z_{sub} (default: 2m), and logarithmic decay between z_{sub} and the ground) is derived for dense canopies from atmospheric wind speed U_a measured at height z_U:

$$U(z) = \begin{cases} U_a \ln\frac{z-d}{z_{0v}} \left[\ln\frac{z_U - d}{z_{0v}}\right]^{-1} & z \geq h \\ U(h) e^{\eta(z/h-1)} & z_{sub} \leq z < h \\ U(z_{sub}) \ln\frac{z}{z_{0g}} \left[\ln\frac{z_{sub}}{z_{0g}}\right]^{-1} & z < z_{sub} \end{cases}$$

where h is stand-scale canopy height (mCH_{50}, Table 1), d = 0.67h is zero-plane displacement, z_{0v} = 0.1h is vegetation roughness length, η is a wind decay factor and z_{0g} is the ground roughness length. In sparse forests with stand-scale canopy cover fraction f_{vs} (= CC_{50}, Table 1), the wind profile (U_{sc}) is obtained as weighted average of the open-site (logarithmic) profile (U_o) and the dense-canopy composite profile (U_{dc}):

$$U_{sc}(z) = f_{vs}^{0.5} U_S(z) + (1 - f_{vs}^{0.5}) U_o(z)$$

Aerodynamic resistances used in the parametrizations of turbulent fluxes are weighted equivalently.

FSM2 is as multi-model framework with a flexible model structure aimed at allowing process representations with different degrees of complexity. In terms of canopy structure representation, the user can choose to either provide all process-specific metrics outlined above, or, alternatively, only canopy height and LAI. While the first option yields optimized hyper-resolution simulations, we reverted to the second option for coarse-resolution simulations following strategy A to create baseline simulations. In this case, LAI-based parametrizations of canopy transmissivity and cover fraction apply:

$$\tau_d = \exp(-0.5\mathrm{LAI})$$

$$f_v = f_{vs} = 1 - \exp(-\mathrm{LAI})$$

All flux parametrizations can be applied as described above, but note that all solar radiation is assumed to be diffuse (i.e. $SW_s = (1 - \alpha_s)\tau_b SW_{\downarrow}$) and near and distant canopy elements are not discerned (i.e. $\tau_{nc} = \tau_d$, $\tau_{fc} = 1$).

Model upscaling from point to grid cell

Hyper- and coarse-resolution simulations both use the same process parametrizations as described above, i.e. no changes occur in the physics of the process parameterizations used. Yet, coarse-resolution simulations require spatially aggregated canopy descriptors and rely on assumptions of unresolved spatial heterogeneity in both canopy structure and snow cover properties.

While aggregation of canopy structure descriptors into grid-cell scale values by arithmetic averaging is straightforward and only affects the input to FSM2, treatment of snowpack heterogeneity required the structure of FSM2 to be altered in order to include a fractional snow cover in energy balance calculations.

For a coarse grid cell with partial snow cover, the energy flux available for melt q_{Melt} [W m^{-2}] found by solving the energy balance at each time step is only applied to the snow-covered fraction f_{snow} [-] of the cell. The rate of change in area-average SWE [kg m^{-2}] is then

$$\frac{dSWE}{dt} = f_{snow} \frac{q_{Melt}}{L_f},$$

where L_f [J kg^{-1}] is the latent heat of fusion. This differs from point-scale calculations, which assume $f_{snow} = 1$ whenever there is snow on the ground.

References

Abe, M., Takata, K., Kawamiya, M., & Watanabe, S. (2017). Vegetation masking effect on future warming and snow albedo feedback in a boreal forest region of northern Eurasia according to MIROC-ESM. *Journal of Geophysical Research: Atmospheres*, *122*(17), 9245–9261. https://doi.org/10.1002/2017JD026957

694 Barnhart, T. B., Molotch, N. P., Livneh, B., Harpold, A. A., Knowles, J. F., & Schneider, D. (2016).
695 Snowmelt rate dictates streamflow: Snowmelt Rate Dictates Streamflow. *Geophysical Research*
696 *Letters*, *43*(15), 8006–8016. https://doi.org/10.1002/2016GL069690

697 Bartlett, P. A., & Verseghy, D. L. (2015). Modified treatment of intercepted snow improves the simulated
698 forest albedo in the Canadian Land Surface Scheme. *Hydrological Processes*, *29*(14), 3208–3226.
699 https://doi.org/10.1002/hyp.10431

700 Bartlett, P. A., MacKay, M. D., & Verseghy, D. L. (2006). Modified snow algorithms in the Canadian
701 land surface scheme: Model runs and sensitivity analysis at three boreal forest stands.
702 *Atmosphere-Ocean*, *44*(3), 207–222. https://doi.org/10.3137/ao.440301

703 Best, M. J., Pryor, M., Clark, D. B., Rooney, G. G., Essery, R. L. H., Ménard, C. B., et al. (2011). The
704 Joint UK Land Environment Simulator (JULES), model description – Part 1: Energy and water
705 fluxes. *Geoscientific Model Development*, *4*(3), 677–699. https://doi.org/10.5194/gmd-4-677-2011

706 Bewley, D., Essery, R., Pomeroy, J. and Ménard, C. (2010) Measurements and modelling of snowmelt and
707 turbulent heat fluxes over shrub tundra. *Hydrology and Earth System Sciences 14*, 1331-1340.
708 https://doi.org/10.5194/hess-14-1331-2010

709 Bloeschl, G. (1999). Scaling issues in snow hydrology. *Hydrological Processes*, *13*, 27.

710 Boone, A., Samuelsson, P., Gollvik, S., Napoly, A., Jarlan, L., Brun, E., & Decharme, B. (2017). The
711 interactions between soil–biosphere–atmosphere land surface model with a multi-energy balance
712 (ISBA-MEB) option in SURFEXv8 – Part 1: Model description. *Geoscientific Model*
713 *Development*, *10*(2), 843–872. https://doi.org/10.5194/gmd-10-843-2017

714 Broxton, P. D., Harpold, A. A., Biederman, J. A., Troch, P. A., Molotch, N. P., & Brooks, P. D. (2015).
715 Quantifying the effects of vegetation structure on snow accumulation and ablation in mixed-
716 conifer forests. *Ecohydrology*, *8*(6), 1073–1094. https://doi.org/10.1002/eco.1565

717 Broxton, P. D., & van Leeuwen, W. J. D. (2020). Structure from Motion of Multi-Angle RPAS Imagery
718 Complements Larger-Scale Airborne Lidar Data for Cost-Effective Snow Monitoring in Mountain
719 Forests. *Remote Sensing*, *12*(14), 2311. https://doi.org/10.3390/rs12142311

720 Clark, M. P., Hendrikx, J., Slater, A. G., Kavetski, D., Anderson, B., Cullen, N. J., et al. (2011).
721 Representing spatial variability of snow water equivalent in hydrologic and land-surface models:
722 A review. *Water Resources Research*, *47*(7). https://doi.org/10.1029/2011WR010745

723 Contosta, A. R., Casson, N. J., Garlick, S., Nelson, S. J., Ayres, M. P., Burakowski, E. A., et al. (2019).
724 Northern forest winters have lost cold, snowy conditions that are important for ecosystems and
725 human communities. *Ecological Applications*, *29*(7). https://doi.org/10.1002/eap.1974

726 Cristea, N. C., Lundquist, J. D., Loheide, S. P., Lowry, C. S., & Moore, C. E. (2014). Modelling how
727 vegetation cover affects climate change impacts on streamflow timing and magnitude in the
728 snowmelt-dominated upper Tuolumne Basin, Sierra Nevada. *Hydrological Processes*, *28*(12),
729 3896–3918. https://doi.org/10.1002/hyp.9909

730 Currier, W. R., & Lundquist, J. D. (2018). Snow Depth Variability at the Forest Edge in Multiple Climates
731 in the Western United States. *Water Resources Research*, *54*(11), 8756–8773.
732 https://doi.org/10.1029/2018WR022553

733 Currier, W. R., Pflug, J., Mazzotti, G., Jonas, T., Deems, J. S., Bormann, K. J., et al. (2019). Comparing
734 Aerial Lidar Observations with Terrestrial Lidar and Snow-Probe Transects From NASA's 2017
735 SnowEx Campaign. *Water Resources Research*, *55*(7), 6285–6294.
736 https://doi.org/10.1029/2018WR024533

737 Dai, Y., Dickinson, R. E., & Wang, Y.-P. (2004). A Two-Big-Leaf Model for Canopy Temperature,
738 Photosynthesis, and Stomatal Conductance. *Journal of Climate*, *17*, 19p.
739 https://doi.org/10.1175/1520-0442(2004)017<2281:ATMFCT>2.0.CO;2

DeBeer, C. M., & Pomeroy, J. W. (2017). Influence of snowpack and melt energy heterogeneity on snow cover depletion and snowmelt runoff simulation in a cold mountain environment. *Journal of Hydrology*, *553*, 199–213. https://doi.org/10.1016/j.jhydrol.2017.07.051

Derksen, C., & Brown, R. (2012). Spring snow cover extent reductions in the 2008–2012 period exceeding climate model projections. *Geophysical Research Letters*, *39*(19). https://doi.org/10.1029/2012GL053387

Dickerson-Lange, S. E., Lutz, J. A., Gersonde, R., Martin, K. A., Forsyth, J. E., & Lundquist, J. D. (2015). Observations of distributed snow depth and snow duration within diverse forest structures in a maritime mountain watershed. *Water Resources Research*, *51*(11), 9353–9366. https://doi.org/10.1002/2015WR017873

Dickerson-Lange, S. E., Gersonde, R. F., Hubbart, J. A., Link, T. E., Nolin, A. W., Perry, G. H., et al. (2017). Snow disappearance timing is dominated by forest effects on snow accumulation in warm winter climates of the Pacific Northwest, United States. *Hydrological Processes*, *31*(10), 1846–1862. https://doi.org/10.1002/hyp.11144

Ellis, C. R., Pomeroy, J. W., & Link, T. E. (2013). Modeling increases in snowmelt yield and desynchronization resulting from forest gap-thinning treatments in a northern mountain headwater basin. *Water Resources Research*, *49*(2), 936–949. https://doi.org/10.1002/wrcr.20089

Essery, R. (2015). A factorial snowpack model (FSM 1.0). *Geoscientific Model Development*, *8*(12), 3867–3876. https://doi.org/10.5194/gmd-8-3867-2015

Essery, R., Bunting, P., Rowlands, A., Rutter, N., Hardy, J., Melloh, R., et al. (2008). Radiative Transfer Modeling of a Coniferous Canopy Characterized by Airborne Remote Sensing. *Journal of Hydrometeorology*, *9*(2), 228–241. https://doi.org/10.1175/2007JHM870.1

Essery, R., Rutter, N., Pomeroy, J., Baxter, R., Stähli, M., Gustafsson, D., et al. (2009). SNOWMIP2: An Evaluation of Forest Snow Process Simulations. *Bulletin of the American Meteorological Society*, *90*(8), 1120–1136. https://doi.org/10.1175/2009BAMS2629.1

Essery, R., Morin, S., Lejeune, Y., & Ménard, C. (2013). A comparison of 1701 snow models using observations from an alpine site. *Advances in Water Resources*, *55*, 131–148. https://doi.org/10.1016/j.advwatres.2012.07.013

Faroux, S., Kaptué Tchuenté, A. T., Roujean, J.-L., Masson, V., Martin, E., & Le Moigne, P. (2013). ECOCLIMAP-II/Europe: a twofold database of ecosystems and surface parameters at 1 km resolution based on satellite information for use in land surface, meteorological and climate models. *Geoscientific Model Development*, *6*(2), 563–582. https://doi.org/10.5194/gmd-6-563-2013

Förster, K., Garvelmann, J., Meißl, G., & Strasser, U. (2018). Modelling forest snow processes with a new version of WaSiM. *Hydrological Sciences Journal*, *63*(10), 1540–1557. https://doi.org/10.1080/02626667.2018.1518626

Gauthier, S., Bernier, P., Kuuluvainen, T., Shvidenko, A.Z., Schepaschenko, D.G., 2015. Boreal forest health and global change. *Science 349*, 819–822. https://doi.org/10.1126/science.aaa9092

Garen, D. C., & Marks, D. (2005). Spatially distributed energy balance snowmelt modelling in a mountainous river basin: estimation of meteorological inputs and verification of model results. *Journal of Hydrology*, *315*(1–4), 126–153. https://doi.org/10.1016/j.jhydrol.2005.03.026

Gichamo, T. Z., & Tarboton, D. G. (2020). UEB parallel: Distributed snow accumulation and melt modeling using parallel computing. *Environmental Modelling & Software*, *125*, 104614. https://doi.org/10.1016/j.envsoft.2019.104614

Gouttevin, I., Lehning, M., Jonas, T., Gustafsson, D., & Mölder, M. (2015). A two-layer canopy model with thermal inertia for an improved snowpack energy balance below needleleaf forest (model SNOWPACK, version 3.2.1, revision 741). *Geoscientific Model Development*, *8*(8), 2379–2398. https://doi.org/10.5194/gmd-8-2379-2015

Harpold, A. A., Guo, Q., Molotch, N., Brooks, P. D., Bales, R., Fernandez-Diaz, J. C., et al. (2014). LiDAR-derived snowpack data sets from mixed conifer forests across the Western United States. *Water Resources Research*, *50*(3), 2749–2755. https://doi.org/10.1002/2013WR013935

Harpold, A. A., Krogh, S. A., Kohler, M., Eckberg, D., Greenberg, J., Sterle, G., & Broxton, P. D. (2020). Increasing the efficacy of forest thinning for snow using high-resolution modeling: A proof of concept in the Lake Tahoe Basin, California, USA. *Ecohydrology*, *13*(4). https://doi.org/10.1002/eco.2203

Hedstrom, N. R., & Pomeroy, J. W. (1998). Measurements and modelling of snow interception in the boreal forest. *Hydrological Processes*, *12*, 15. https://doi.org/10.1002/(SICI)1099-1085(199808/09)12:10/11<1611::AID-HYP684>3.0.CO;2-4.

Hock, R., Rasul, G., Adler, C., Cáceres, B., Gruber, S., Hirabayashi, Y., Jackson, M., et al. (2019).: High Mountain Areas. In: IPCC Special Report on the Ocean and Cryosphere in a Changing Climate. H.-O. Pörtner, D.C. Roberts, V. Masson-Delmotte, P. Zhai, M. Tignor, E. Poloczanska, K. Mintenbeck, A. Alegría, M. Nicolai, A. Okem, J. Petzold, B. Rama, N.M. Weyer (eds.). *In press.*

Jonas, T., Webster, C., Mazzotti, G., & Malle, J. (2020). HPEval: A canopy shortwave radiation transmission model using high-resolution hemispherical images. *Agricultural and Forest Meteorology*, *284*, 107903. https://doi.org/10.1016/j.agrformet.2020.107903

Kostadinov, T. S., Schumer, R., Hausner, M., Bormann, K. J., Gaffney, R., McGwire, K., et al. (2019). Watershed-scale mapping of fractional snow cover under conifer forest canopy using lidar. *Remote Sensing of Environment*, *222*, 34–49. https://doi.org/10.1016/j.rse.2018.11.037

Krogh, S. A., Broxton, P. D., Manley, P. N., & Harpold, A. A. (2020). Using Process Based Snow Modeling and Lidar to Predict the Effects of Forest Thinning on the Northern Sierra Nevada Snowpack. *Frontiers in Forests and Global Change*, *3*, 21. https://doi.org/10.3389/ffgc.2020.00021

Lawler, R. R., & Link, T. E. (2011). Quantification of incoming all-wave radiation in discontinuous forest canopies with application to snowmelt prediction. *Hydrological Processes*, *25*(21), 3322–3331. https://doi.org/10.1002/hyp.8150

Liston, G. E. (2004). Representing Subgrid Snow Cover Heterogeneities in Regional and Global Models. *Journal of Climate*, *17*, 17. https://doi.org/10.1175/1520-0442(2004)017<1381:RSSCHI>2.0.CO;2

Luce, C. H., Tarboton, D. G., & Cooley, K. R. (1999). Sub-grid parameterization of snow distribution for an energy and mass balance snow cover model. *Hydrological Processes*, *13*, 13p. https://doi.org/10.1002/(SICI)1099-1085(199909)13:12/13<1921::AID-HYP867>3.0.CO;2-S

Lundquist, J. D., Dickerson-Lange, S. E., Lutz, J. A., & Cristea, N. C. (2013). Lower forest density enhances snow retention in regions with warmer winters: A global framework developed from plot-scale observations and modeling: Forests and Snow Retention. *Water Resources Research*, *49*(10), 6356–6370. https://doi.org/10.1002/wrcr.20504

Magnusson, J., Eisner, S., Huang, S., Lussana, C., Mazzotti, G., Essery, R., et al. (2019). Influence of Spatial Resolution on Snow Cover Dynamics for a Coastal and Mountainous Region at High Latitudes (Norway). *Water Resources Research*, *55*(7), 5612–5630. https://doi.org/10.1029/2019WR024925

Mahat, V., Tarboton, D. G., & Molotch, N. P. (2013). Testing above- and below-canopy representations of turbulent fluxes in an energy balance snowmelt model. *Water Resources Research*, *49*(2), 1107–1122. https://doi.org/10.1002/wrcr.20073

Malle, J., Rutter, N., Mazzotti, G., & Jonas, T. (2019). Shading by Trees and Fractional Snow Cover Control the Subcanopy Radiation Budget. *Journal of Geophysical Research: Atmospheres*, *124*(6), 3195–3207. https://doi.org/10.1029/2018JD029908

Mazzotti, G., Currier, W. R., Deems, J. S., Pflug, J. M., Lundquist, J. D., & Jonas, T. (2019a). Revisiting Snow Cover Variability and Canopy Structure Within Forest Stands: Insights from Airborne Lidar Data. *Water Resources Research*, *55*(7), 6198–6216. https://doi.org/10.1029/2019WR024898

Mazzotti, G., Malle, J., Barr, S., & Jonas, T. (2019b). Spatially Continuous Characterization of Forest Canopy Structure and Subcanopy Irradiance Derived from Handheld Radiometer Surveys. *Journal of Hydrometeorology*, *20*(7), 1417–1433. https://doi.org/10.1175/JHM-D-18-0158.1

Mazzotti, G., Essery, R., Moeser, C. D., & Jonas, T. (2020a). Resolving Small-Scale Forest Snow Patterns Using an Energy Balance Snow Model with a One-Layer Canopy. *Water Resources Research*, *56*(1), e2019WR026129. https://doi.org/10.1029/2019WR026129

Mazzotti, G., Essery, R., Webster, C., Malle, J., & Jonas, T. (2020b). Process-level evaluation of a hyper-resolution forest snow model using distributed multi-sensor observations. *Water Resources Research*, *n/a*(n/a), e2020WR027572. https://doi.org/10.1029/2020WR027572

Meredith, M., Sommerkorn, M., Cassotta, S., Derksen, C., Ekaykin, A., Hollowed, A., Kofinas, G., et al. (2019) Polar Regions. In: IPCC Special Report on the Ocean and Cryosphere in a Changing Climate. H.-O. Pörtner, D.C. Roberts, V. Masson-Delmotte, P. Zhai, M. Tignor, E. Poloczanska, K. Mintenbeck, A. Alegría, M. Nicolai, A. Okem, J. Petzold, B. Rama, N.M. Weyer (eds.). In press.

Moeser, D., Roubinek, J., Schleppi, P., Morsdorf, F., & Jonas, T. (2014). Canopy closure, LAI and radiation transfer from airborne LiDAR synthetic images. *Agricultural and Forest Meteorology*, *197*, 158–168. https://doi.org/10.1016/j.agrformet.2014.06.008

Moeser, D., Stähli, M., & Jonas, T. (2015a). Improved snow interception modeling using canopy parameters derived from airborne LiDAR data. *Water Resources Research*, *51*(7), 5041–5059. https://doi.org/10.1002/2014WR016724

Moeser, D., Morsdorf, F., & Jonas, T. (2015b). Novel forest structure metrics from airborne LiDAR data for improved snow interception estimation. *Agricultural and Forest Meteorology*, *208*, 40–49. https://doi.org/10.1016/j.agrformet.2015.04.013

Moeser, D., Mazzotti, G., Helbig, N., & Jonas, T. (2016). Representing spatial variability of forest snow: Implementation of a new interception model. *Water Resources Research*, *52*(2), 1208–1226. https://doi.org/10.1002/2015WR017961

Mote, P. W., Li, S., Lettenmaier, D. P., Xiao, M., & Engel, R. (2018). Dramatic declines in snowpack in the western US. *Climate and Atmospheric Science*, *1*(1), 1–6. https://doi.org/10.1038/s41612-018-0012-1Musselman, K. N., Molotch, N. P., Margulis, S. A., Lehning, M., & Gustafsson, D. (2012a). Improved snowmelt simulations with a canopy model forced with photo-derived direct beam canopy transmissivity. *Water Resources Research*, *48*(10). https://doi.org/10.1029/2012WR012285

Musselman, K. N., Molotch, N. P., Margulis, S. A., Kirchner, P. B., & Bales, R. C. (2012b). Influence of canopy structure and direct beam solar irradiance on snowmelt rates in a mixed conifer forest. *Agricultural and Forest Meteorology*, *161*, 46–56. https://doi.org/10.1016/j.agrformet.2012.03.011

Ni-Meister, W., Yang, W., & Kiang, N. Y. (2010). A clumped-foliage canopy radiative transfer model for a global dynamic terrestrial ecosystem model. I: Theory. *Agricultural and Forest Meteorology*, *150*(7–8), 881–894. https://doi.org/10.1016/j.agrformet.2010.02.009

Oleson, K. W., Lawrence, D. M., Bonan, G. B., Drewniak, B., Huang, M., Levis, S., et al. (2013). Technical Description of version 4.5 of the Community Land Model (CLM). *NCAR Technical Note 434*. https://doi.org/10.5065/D6RR1W7M.

Painter, T. H., Berisford, D. F., Boardman, J. W., Bormann, K. J., Deems, J. S., Gehrke, F., et al. (2016). The Airborne Snow Observatory: Fusion of scanning lidar, imaging spectrometer, and physically-

based modeling for mapping snow water equivalent and snow albedo. *Remote Sensing of Environment*, *184*, 139–152. https://doi.org/10.1016/j.rse.2016.06.018

Pearson, R. G., Phillips, S. J., Loranty, M. M., Beck, P. S. A., Damoulas, T., Knight, S. J., & Goetz, S. J. (2013). Shifts in Arctic vegetation and associated feedbacks under climate change. *Nature Climate Change*, *3*(7), 673–677. https://doi.org/10.1038/nclimate1858

Pflug, J. M., & Lundquist, J. D. (2020). Inferring Distributed Snow Depth by Leveraging Snow Pattern Repeatability: Investigation Using 47 Lidar Observations in the Tuolumne Watershed, Sierra Nevada, California. *Water Resources Research*, *56*(9), e2020WR027243. https://doi.org/10.1029/2020WR027243

Reid, T. D., Essery, R. L. H., Rutter, N., & King, M. (2013). Data-driven modelling of shortwave radiation transfer to snow through boreal birch and conifer canopies. *Hydrological Processes*, n/a-n/a. https://doi.org/10.1002/hyp.9849

Roth, T. R., & Nolin, A. W. (2017). Forest impacts on snow accumulation and ablation across an elevation gradient in a temperate montane environment. *Hydrology and Earth System Sciences*, *21*(11), 5427–5442. https://doi.org/10.5194/hess-21-5427-2017

Rutter, N., Essery, R., Pomeroy, J., Altimir, N., Andreadis, K., Baker, I., et al. (2009). Evaluation of forest snow processes models (SnowMIP2). *Journal of Geophysical Research*, *114*(D6), D06111. https://doi.org/10.1029/2008JD011063

Sicart, J. E., Pomeroy, J. W., Essery, R. L. H., Hardy, J., Link, T., & Marks, D. (2004). A Sensitivity Study of Daytime Net Radiation during Snowmelt to Forest Canopy and Atmospheric Conditions. *Journal of Hydrometeorology*, *5*, 12. https://doi.org/10.1175/1525-7541(2004)005<0774:ASSODN>2.0.CO;2

Sorensen, P. O., Templer, P. H., Christenson, L., Duran, J., Fahey, T., Fisk, M. C., et al. (2016). Reduced snow cover alters root-microbe interactions and decreases nitrification rates in a northern hardwood forest. *Ecology*, *97*(12), 3359–3368. https://doi.org/10.1002/ecy.1599

Stähli, M., Jonas, T. and D. Gustafsson (2009) The role of snow interception in winter-time radiation processes of a coniferous sub-alpine forest. *Hydrological Processes*, *23*, 2498-2512. https://doi.org/10.1002/hyp.7180al.

Sturm, M., Goldstein, M. A., & Parr, C. (2017). Water and life from snow: A trillion dollar science question. *Water Resources Research*, *53*(5), 3534–3544. https://doi.org/10.1002/2017WR020840

Sun, N., Wigmosta, M., Zhou, T., Lundquist, J., Dickerson-Lange, S., & Cristea, N. (2018). Evaluating the functionality and streamflow impacts of explicitly modelling forest-snow interactions and canopy gaps in a distributed hydrologic model. *Hydrological Processes*, *32*(13), 2128–2140. https://doi.org/10.1002/hyp.13150

Swenson, S. C., & Lawrence, D. M. (2012). A new fractional snow-covered area parameterization for the Community Land Model and its effect on the surface energy balance. *Journal of Geophysical Research: Atmospheres*, *117*(D21), n/a-n/a. https://doi.org/10.1029/2012JD018178

Thackeray, C. W., Fletcher, C. G., & Derksen, C. (2014). The influence of canopy snow parameterizations on snow albedo feedback in boreal forest regions: Boreal forest snow albedo feedback. *Journal of Geophysical Research: Atmospheres*, *119*(16), 9810–9821. https://doi.org/10.1002/2014JD021858

Todt, M., Rutter, N., Fletcher, C. G., & Wake, L. M. (2019). Simulated single-layer forest canopies delay Northern Hemisphere snowmelt. *The Cryosphere*, *13*(11), 3077–3091. https://doi.org/10.5194/tc-13-3077-2019

Trujillo, E., Ramírez, J. A., & Elder, K. J. (2009). Scaling properties and spatial organization of snow depth fields in sub-alpine forest and alpine tundra. *Hydrological Processes*, *23*(11), 1575–1590. https://doi.org/10.1002/hyp.7270

928 Varhola, A., Coops, N. C., Weiler, M., & Moore, R. D. (2010). Forest canopy effects on snow
929 accumulation and ablation: An integrative review of empirical results. *Journal of Hydrology*,
930 *392*(3–4), 219–233. https://doi.org/10.1016/j.jhydrol.2010.08.009

931 Viviroli, D., & Weingartner, R. (2004). The hydrological significance of mountains: from regional to
932 global scale. *Hydrology and Earth System Sciences*, *8*(6), 1017–1030.
933 https://doi.org/10.5194/hess-8-1017-2004

934 Viviroli, D., Archer, D. R., Buytaert, W., Fowler, H. J., Greenwood, G. B., Hamlet, A. F., et al. (2011).
935 Climate change and mountain water resources: overview and recommendations for research,
936 management and policy. *Hydrology and Earth System Sciences*, *15*(2), 471–504.
937 https://doi.org/10.5194/hess-15-471-2011

938 Webster, C., Rutter, N., Zahner, F., & Jonas, T. (2016a). Measurement of Incoming Radiation below
939 Forest Canopies: A Comparison of Different Radiometer Configurations. *Journal of*
940 *Hydrometeorology*, *17*(3), 853–864. https://doi.org/10.1175/JHM-D-15-0125.1

941 Webster, C., Rutter, N., Zahner, F., & Jonas, T. (2016b). Modeling subcanopy incoming longwave
942 radiation to seasonal snow using air and tree trunk temperatures. *Journal of Geophysical*
943 *Research: Atmospheres*, *121*(3), 1220–1235. https://doi.org/10.1002/2015JD024099

944 Webster, C., Mazzotti, G., Essery, R., & Jonas, T. (2020). Enhancing airborne LiDAR data for improved
945 forest structure representation in shortwave transmission models. *Remote Sensing of Environment*,
946 *249*, 112017. https://doi.org/10.1016/j.rse.2020.112017

947 Widlowski, J.-L., Mio, C., Disney, M., Adams, J., Andredakis, I., Atzberger, C., et al. (2015). The fourth
948 phase of the radiative transfer model intercomparison (RAMI) exercise: Actual canopy scenarios
949 and conformity testing. *Remote Sensing of Environment*, *169*, 418–437.
950 https://doi.org/10.1016/j.rse.2015.08.016

951 Wipf, S., & Rixen, C. (2010). A review of snow manipulation experiments in Arctic and alpine tundra
952 ecosystems. *Polar Research*, *29*(1), 95–109. https://doi.org/10.1111/j.1751-8369.2010.00153.x

953 Yuan, H., Dickinson, R. E., Dai, Y., Shaikh, M. J., Zhou, L., Shangguan, W., & Ji, D. (2014). A 3D
954 Canopy Radiative Transfer Model for Global Climate Modeling: Description, Validation, and
955 Application. *Journal of Climate*, *27*(3), 1168–1192. https://doi.org/10.1175/JCLI-D-13-00155.1